Report Title:	General Single Phase Wellbore Flow Model		

BC/14862-$T/$

Report Type:	TOPICAL	Reporting Period Start Date:	End Date:

Principal Author(s): Liang-Biao Ouyang
Sepehr Arbabi
Khalid Aziz

$DOE/BC/14862--TI$

Report Issue Date:	02/05/1997	DOE Award No.: DE- FG22 -93BC14862

Submitting Organization(s) Name & Address

Department of Petroleum Engineering
Stanford University
Stanford, CA 94305-2220

(1)

RECEIVED

APR 0 7 1997

OSTI

(2)

(3)

(4)

MASTER

(5)

DISCLAIMER

Portions of this document may be illegible in electronic image products. Images are produced from the best available original document.

Disclaimer

Abstract

A general wellbore flow model, which incorporates not only frictional, accelerational and gravitational pressure drops, but also the pressure drop caused by inflow, is presented in this report. The new wellbore model is readily applicable to any wellbore perforation patterns and well completions, and can be easily incorporated in reservoir simulators or analytical reservoir inflow models.

Three dimensionless numbers, the accelerational to frictional pressure gradient ratio R_{af}, the gravitational to frictional pressure gradient ratio R_{gf}, and the inflow-directional to accelerational pressure gradient ratio R_{da}, have been introduced to quantitatively describe the relative importance of different pressure gradient components. For fluid flow in a production well, it is expected that there may exist up to three different regions of the wellbore: the laminar flow region, the partially-developed turbulent flow region, and the fully-developed turbulent flow region. The laminar flow region is located near the well toe, the partially-turbulent flow region lies in the middle of the wellbore, while the fully-developed turbulent flow region is at the downstream end or the heel of the wellbore. Length of each region depends on fluid properties, wellbore geometry and flow rate. As the distance from the well toe increases, flow rate in the wellbore increases and the ratios R_{af} and R_{da} decrease. Consequently accelerational and inflow-directional pressure drops have the greatest impact in the toe region of the wellbore. Near the well heel the local wellbore flow rate becomes large and close to the total well production rate, here R_{af} and R_{da} are small, therefore, both the accelerational and inflow-directional pressure drops can be neglected.

It is found that the influence of either inflow or outflow depends on the flow regime present in the wellbore. For laminar flow, wall friction increases due to inflow but decreases due to outflow. For turbulent flow, inflow reduces the wall friction, while outflow increases it. To obtain the precise contribution of the frictional pressure drop along the wellbore, new wall friction factor correlations for pipe flow with perforation influx have been developed based on the published research work and the Stanford horizontal well experimental data. They can be applied in wellbore flow to determine wall friction shear and frictional pressure drop for either inflow (production well) or outflow (injection well) and for either laminar flow or turbulent flow.

The new wellbore flow model has been used to study the relative importance of frictional and accelerational components of pressure drop along a horizontal well. Other sensitivity analyses have also been conducted. Moreover, the new wellbore model has been coupled with a reservoir model to study the performance of a horizontal well. Calculations show that the accelerational pressure gradient may or may not be important compared to the frictional component depending on the specific pipe geometry, fluid properties and flow conditions. It is recommended that the new wellbore flow model be included in wellbore-reservoir coupling models to achieve more accurate predictions of pressure drop and inflow distribution along the wellbore as well as well production or injection rates.

Contents

List of Figures

1. Introduction

Over the last decade horizontal wells have become a well–established technology for the recovery of oil and gas. Considerable amount of analytical and experimental work has been published on various aspects of horizontal well production, including transient flow models, stabilized inflow models, productivity indices, and cresting behavior. Although these methods provide insight into the behaviors of horizontal wells, few of them considers pressure drop along the wellbore and essentially infinite conductivity is assumed. In 1990 Dikken [1] proposed the first semi-analytical model to evaluate the production performance of a horizontal well with the consideration of the wellbore pressure drop resulting from turbulent flow. Since then, Islam & Chakma [2], Folefac et al. [3], Briggs [4], Ozkan et al. [5], Ihara et al. [6], Seines et al. [7], Landman [8], Novy [9] and other researchers have presented different coupling models for wellbore flow and reservoir inflow through perforations. However, even in cases where pressure drop along a wellbore is considered, only the frictional component is included, pressure drop due to accelerational and other effects is usually neglected. As we show in this report, due to the existence of perforation inflow, the accelerational pressure drop can be important relative to the frictional part and can significantly influence the well flow rates under some flow conditions. Furthermore, traditional methods to determine frictional pressure drop in pipe flow that do not account for inflow or outflow effect are employed in most of the coupling models, which is not justified since inflow changes the wall friction in the wellbore.

A general wellbore flow model, which incorporates not only frictional, accelerational and gravitational pressure drops, but also the pressure drop caused by inflow, is presented in this report. The new model is readily applicable to any wellbore perforation pattern and well completion, and can be easily incorporated in reservoir simulators or analytical reservoir inflow models. To calculate precisely the contribution of frictional pressure drop along the wellbore, new wall friction factor correlations for pipe flow with perforation influx are also developed based on some published research work and the Stanford horizontal wellbore experimental data. They can be applied in wellbore flow to determine wall friction shear and frictional pressure drop for either inflow (production well) or outflow (injection well) and for either laminar or turbulent flow.

The new wellbore flow model has been used to study the relative importance of frictional and accelerational components of pressure drop along a horizontal well. Other sensitivity analyses have also been conducted. Moreover, the new wellbore model has been coupled with a simple reservoir model to study the performance of different horizontal wells.

2. Literature Review

As an effective boundary layer control method, fluid flow in channels or pipes with fluid injection or extraction through the wall surface was first investigated by mechanical engineers as early as 1904 (Schilichting, [10]). Early researchers only focused on fluid flow past a flat surface with injection or suction in a part of the whole surface. Study of this aspect is of great practical importance for the aerospace industry and it has enhanced the design of aeroplanes and improved their performance. For example, only a little suction on the surface of an airfoil was found to significantly increase lift and decrease drag, as well as alter the heat transfer behavior. This discovery has been applied in the aerospace and other related industries, such as chemical industry (membrane filtration [11], transpiration cooling [12]), and nuclear industry (the enrichment of U_{235} [13]). Surprisingly, more than 50 years had passed since the work on flat plates before Yuan & Finkelstein [14] investigated laminar fluid flow in pipes in the presence of fluid injection or extraction through the porous wall.

Most theoretical studies for the friction factor and heat transfer characteristics for laminar pipe flow with mass transfer through the porous wall are based on similarity solutions where the velocity and temperature profiles are functions only of the radial coordinate that stay unchanged in the axial direction. Similarity solutions have been found to exist in a certain range of the wall Reynolds number R_{ew} (injection Reynolds number for injection case and extraction or suction Reynolds number for suction case) but not for other values.

Yuan & Finkelstein [14] were the first to investigate the effect of uniform injection and suction at the pipe wall on the two-dimensional steady-state laminar flow of a fluid in a porous pipe by solving the Navier-Stokes equations in cylindrical coordinates for both very large and very small inflow Reynolds number cases. The dynamic equations were reduced by means of similarity analysis to a third-order nonlinear ordinary differential equation with appropriate boundary conditions, which was then solved by a perturbation method. The results show that the effect of injection at the pipe wall is to increase the wall friction shear and thus increase the friction factor while suction decreases them. Kinney [15] examined the frictional and heat-transfer charateristics of fully-developed laminar flow in porous pipe by utilizing numerical solutions of the momentum and energy equations. The fluid flow in a straight circular tube with uniform inflow or outflow was considered. The corresponding Navier-Stokes equations were reduced to an ordinary differential form also by applying similarity analysis. Olson & Eckert [16] performed experimental studies of turbulent air flow in a porous circular pipe with uniform air injection through the pipe wall. The fully-developed turbulent air flow at Reynolds number of 28,000 to 82,000 entered the pipe while air was injected uniformly through the wall at various ratios of injection velocity to the average velocity at the entrance, ranging from 0.00246 to 0.0584. Kinney & Sparrow [17] presented results for frictional, heat-transfer and mass-transfer characteristics of fully-developed turbulent flow in pipes with suction. They assumed that the velocity and temperature fields are locally self-similar. The variation of the friction factor with the relative suction velocity $\frac{V_w}{U}$ was given in graphical form for parametric values of the Reynolds number. Merkin et al. [18] extended these results to account for the effect of suction on the turbulence level in the fluid (suction decreases turbulence level). Their results show good agreement with the measurements of the velocity profiles by Weissberg & Berman [19]. Unfortunately, no results of the friction factor

5

were given. By modifying the Kinney & Sparrow's analysis [17] , Doshi & Gill [20] obtained an excellent agreement with the experimental velocity profiles of Weissberg & Berman [19]. Lombardi et al. [21] investigated the fully developed turbulent flow along a pipe with air injection through the porous wall and found that the Nusselt number in the downstream region of the pipe could be related by the local parameters, such as the local axial flow Reynolds number and the injection Reynolds number, without separate dependence upon the inlet axial Reynolds number and axial position.

It is quite interesting to note that the flow characterisics of pipe flow with mass transfer through pipe wall are different from those of channel flow or flow past a flat plate. For example, considering the laminar flow case, the local friction factor increases with an increase of inflow Reynolds number for pipe flow but decreases for channel flow. Moreover, the suction-induced transition to turbulent flow (suction-induced instability) and the existence of multiple solutions for pipe flow have no counterpart in channel flow (Raithby, [22]).

Another interesting fact is the different behavior of the local friction factor change with the inflow rates for laminar flow and for turbulent flow. For laminar flow, the local friction factor increases with an increase in the injection Reynolds number, whereas it decreases for turbulent flow. The underlying mechanisms will be discussed later in this report.

The fluid flow in a pipe with mass transfer through pipe wall did not interest petroleum engineers until the horizontal well technology was introduced and widely applied in the petroleum industry starting in the 1980s. For fluid flow in horizontal wells, the flow format is quite similar to the pipe flow with mass transfer through porous wall. The main differences between these two types of flow are as follows:

- In horizontal wells, the mass transfer is normally through perforations, while in the case of pipe flow it is through pores in the wall. In other words, the effective perforation density is very large (theoretically infinite) for the porous pipe flow case. Nevertheless, in the case of openhole completions, the horizontal well and porous pipe flow problems are conceptually identical.

- The injection rates are usually quite small in the porous pipe flow case, this is not necessarily the case for wellbore flow.

- When there is no mass transfer through the pipe wall, the effective pipe roughness is very different from the actual pipe roughness in a horizontal well due to the effect of perforations on the axial flow (such as flow separation, cavity flow or secondary flow), but it changes only slightly from the actual value for the porous pipe flow case.

Little information is available related to the significance of the above-mentioned differences on the prediction of horizontal well behavior. Although much research work has been completed for the porous pipe flow, these results may not be easily applicable to horizontal wells. Recognizing this fact, petroleum engineers began to study the horizontal well flow behavior from the late 1980s.

Kloster [23] experimentally studied flow resistance in a perforated pipe, both with and without flow injection through the pipe wall, by using a pipe of $6\frac{5}{6}$ inch OD and 17-feet in length. The pipe had a perforated section of 14-feet with a perforation density of 180 holes per foot. The Reynolds number covered in this study ranged from $60,000$ to $450,000$. Asheim et al. [24] stated that the total pressure drop along the perforated pipe is made up

6

of wall friction ΔP_{fri} and inflow acceleration and computed the wall friction factor in the same way as for regular unperforated pipe and neglected the second-order term. Ihara et al. [25] studied the channel flow with mass transfer through porous walls, which had continuous influx into the horizontal channel from an oil reservoir model. They stated that the pressure gradients increase almost uniformly in the test channel due to the confluence of influx and axial flow and the pressure drop due to confluence increases linearly with the influx velocity. Islam & Chakma [2] carried out an experimental study for multiphase flow in horizontal lucite tubes of 2.54 cm and 7.6 cm internal diameters with influx points made of 1m stainless steel tubing of 3.2 mm internal diameter. They found that both oil viscosity and void fraction have influence on the transition location from bubble to slug flow. They also found that the pressure drop increases due to the existence of flow through perforations for the oil/gas case, whereas for the oil/water/gas case, the presence of water leads to segregated bubbly oil and water flow, which lowers the wall friction in the lower part of the tube.

Although pipe flow with mass transfer through pipe wall has been the topic of numerous research activities, more work seems necessary considering the following observations:

- No correlations exist for determining the wall friction factors for single phase and multiphase fluid flow in a wellbore with inflow or outflow through perforations.

- The accelerational and inflow-directional pressure drop are neglected in most of the single wellbore flow models or wellbore-reservoir coupling models.

- The wall friction shears are usually evaluated by using the friction factor correlations for pipe flow without mass transfer through pipe wall. Therefore, the impact of mass transfer through pipe wall on the wall friction is not included.

- No mechanistic model has been developed to predict the flow characteristics, such as flow pattern, liquid holdup and pressure drop in multiphase wellbore flow with the presence of inflow or outflow through perforations.

7

3. General Wellbore Flow Model

Consider fluid flow in a wellbore as shown in Figure A.1 and assume single phase flow of an incompressible Newtonian fluid under isothermal conditions with no heat transfer to and from the fluid. Furthermore, assume that no mechanical work is done on or by the fluid during its passage through the pipe. With these assumptions, the momentum balance equation takes the form (see Appendix A for details)

$$
\begin{aligned}
[(pA)_2 - (pA)_1] &= \left[\frac{1}{\alpha_1 g_c} \rho A_1 U_1^2 - \frac{1}{\alpha_2 g_c} \rho A_2 U_2^2 \right] \\
&\quad + \frac{n \triangle x}{\alpha_I g_c} \rho A_I U_r U_x - \tau_w S \triangle x \\
&\quad - \rho \bar{A} \triangle x \frac{g}{g_c} \sin \theta
\end{aligned}
\tag{3.1}
$$

which can be rearranged to get the following pressure gradient equation

$$
\begin{aligned}
\frac{dp}{dx} &= -\frac{\rho}{g_c} \frac{d}{dx} \left(\frac{U^2}{\alpha} \right) - \tau_w \frac{S}{A} \\
&\quad + \frac{n}{\alpha_I g_c} \rho \frac{A_I}{A} U_r U_x - \rho \frac{g}{g_c} \sin \theta
\end{aligned}
\tag{3.2}
$$

Eq. 3.2 indicates that the overall pressure gradient consists of four different components:

- The pressure gradient due to kinetic energy change (accelerational effects). This term should be zero for incompressible fluid flow in pipes of constant ID and without inflow or extraction. Obviously, it will not be zero for wellbore flow with influx.

- The frictional pressure gradient. This part of pressure gradient depends on both axial and perforation flows.

- The pressure gradient due to the inflow direction, and it is termed as inflow-directional pressure drop in this report. It may help or hinder the axial flow depending on the inflow direction.

- The gravitational pressure gradient. It is reasonable to assume that the gravitational pressure gradient is trivial and thus negligible for horizontal wellbore flow.

In order to quantitatively describe the relative importance of different pressure gradient components, the following three dimensionless numbers are introduced:

R_{af} is defined as the ratio of the accelerational pressure gradient and the frictional pressure gradient;

8

R_{gf} is defined as the ratio of the gravitational pressure gradient and the frictional pressure gradient;

R_{da} is defined as the ratio of the directional pressure gradient and the accelerational pressure gradient.

Therefore, the total pressure gradient can be expressed as:

$$\frac{dp}{dx} = -\frac{4\tau_w}{D}[1 + R_{af}(1 - R_{da}) + R_{gf}] \tag{3.3}$$

It is easily seen from Eq. A.14 that the closer we are to the horizontal well toe ($x = 0$), the smaller the local wellbore production rate q_w, thus the larger the R_{af} and the more important the accelerational pressure gradient. In contrast, near the heel of the horizontal well ($x = L$), the local production rate q_w becomes large and close to the total well production rate, while the specific influx (inflow rate per wellbore length) q_e does not change significantly, so R_{af} is small, and the accelerational pressure gradient is small and may be negligible.

For the uniform inflow case, we have shown in Appendix A that:

- In the laminar flow regime ($x \leq L_t$), R_{af} is only dependent on fluid properties, inflow rate and pipe ID, but it is independent of location x and pipe roughness ϵ. The larger the q_e, the larger the R_{af}, but the shorter the laminar flow length L_t.

- In the turbulent flow regime ($x > L_t$), the Fanning friction factor f is dependent on the local Reynolds number, the wall Reynolds number and the relative pipe roughness, as a consequence, the R_{af} depends on location x, pipe geometry (pipe ID and pipe roughness), fluid properties, and inflow rates.

Since turbulent flow occurs along almost the whole wellbore section for most practical situations, it is anticipated that the momentum correction factor α does not change much for different velocity profiles (Ouyang & Aziz, [26]), therefore, α can be assumed constant. Besides, the derivative $\frac{dU}{dx}$ can be obtained from the mass balance equation. Hence, Eq. A.9 can be rewritten as

$$\tau_w = \frac{D}{4}\left[\frac{dp}{dx} - n\frac{A_I}{A}\frac{2\rho}{g_c\alpha}UU_I + n\frac{A_I}{A}\frac{\rho}{2g_c\alpha_I}U_I^2\sin 2\gamma - \rho\frac{g}{g_c}\sin\theta\right] \tag{3.4}$$

Based on Eq. 3.4, the wall friction shear stress and hence the wall friction factor can be calculated. The wall friction factor is expected to depend on the local axial Reynolds number, the injection Reynolds number, the effective relative pipe roughness and maybe the inflow/axial flow rate ratios.

4. Influences of Mass Transfer through Pipe Wall

Based on the discussion detailed in Appendix B, it is found that:

- *Laminar Flow:* when mass transfer through the pipe wall exists, the parabolic velocity profile is inappropriate for describing the velocity distribution over the pipe cross section. The velocity should increase for injection and decrease for suction following the law of mass conservation. Although fluid injection leads to the increasing of axial velocities across the whole pipe section, as can be imagined, the axial velocities near the pipe wall will increase more than those far away from the wall (and thus close to the centerline). Similarly, suction decreases axial velocities near the wall more significantly than those away from the wall. As a result, the velocity gradient on and near the pipe wall increases due to the inflow while it decreases due to outflow. Corrrespondingly, the wall friction increases for inflow case but dcreases for outflow.

- *Turbulent Flow:* with the presence of mass transfer through perforations, the time average velocity profile for turbulent pipe flow is altered due to the interaction between the axial flow and the perforation flow. For the injection case, the inflow lifts and expands the turbulent boundary layer and thus increases the axial velocity beyond the layer while decreases the velocity within the layer to follow the mass conservation law. As a consequence the axial velocity gradient near the pipe wall decreases and so does the wall friction shear stress. On the contrary, the suction lowers and reduces the boundary layer and thus decreases the average velocity outside the layer but increases the velocity inside the layer, which results in an increase of the axial velocity gradient near the pipe wall and hence the wall friction shear stress. The analysis is consistent with the numerical observations of Kinney & Sparrow [17] for pipe flow with suction through pipe wall.

5. New Wall Friction Factor Correlations

As discussed above in the previous section, the mass transfer through the pipe wall affects wall friction shear. The influence of either inflow or outflow depends on the flow regime present in the wellbore. The inflow (injection) increases the wall friction for laminar flow while decreases it for turbulent flow. On the contrary, outflow (suction) decreases the wall friction for laminar flow while increases the friction for turbulent flow. In other words, the wall friction is altered compared to the pipe flow where no inflow or outflow is present. Therefore, the friction factor correlations for pipe flow without inflow or outflow can not be used for wellbore flow with both axial flow in the pipe and inflow or outflow through perforations.

5.1 Laminar Flow in a Porous Pipe

Kinney [15] numerically solved the problem of fully-developed laminar flow in a porous pipe where both axial flow and inflow or outflow through pipe wall were present. The results show that the ratio between the local friction factor f and the no-wall-flow friction factor f_0[1] is only dependent on the wall Reynolds number. Unfortunately, this relationship was given in a graphical form and no equation was supplied. Hence, it cannot be easily used in a wellbore flow model.

Based on the reduced ordinary differential equation for the dimensionless stream-function and the numerical procedure provided in Kinney [15], the ratios between the local friction factor and the no-wall-flow friction factor corresponding to different wall Reynolds numbers R_{ew} were calculated and are shown in Figure 5.1 and Figure 5.2. The prediction of the local wall friction factor by the Yuan & Finkelstein [14] equation is also shown in Figure 5.1. Since Yuan & Finkelstein [14] equation was obtained by means of a perturbation method where the injection wall Reynolds number R_{ew} was assumed sufficiently small, it is anticipated that the Yuan & Finkelstein [14] equation can only be used for small R_{ew} case (say $R_{ew} \leq 2.0$).

These data have also been used to develop the following friction factor correlations by means of a fast and effective nonlinear regression procedure called Polytope method (Gill et al. [27]; Ouyang, [28]).

---

[1]The no-wall-flow friction factor is defined in this report as the friction factor computed from the correlations for pipe flow with no mass transfer through pipe wall by using local Reynolds number and effective pipe roughness.

For laminar flow

$$f_0 = \frac{16.0}{R_e}$$

For turbulent flow

$$f_0^{-0.5} = -4.0 \log \left[\frac{\epsilon}{3.7D} + \frac{1.255}{f_0^{0.5} R_e} \right]$$

- For inflow (injection) case

$$f = \frac{16.0}{R_e}\left(1 + 0.04304R_{ew}^{0.6142}\right) \tag{5.1}$$

- For outflow (suction or extraction) case

$$f = \frac{16.0}{R_e}\left[1 - 0.0625\frac{(-R_{ew})^{1.3056}}{(R_{ew} + 4.626)^{-0.2724}}\right] \tag{5.2}$$

Comparisons between friction factors predicted by the new correlations and published numerical experiments are also shown in both Figures 5.1 and 5.2.
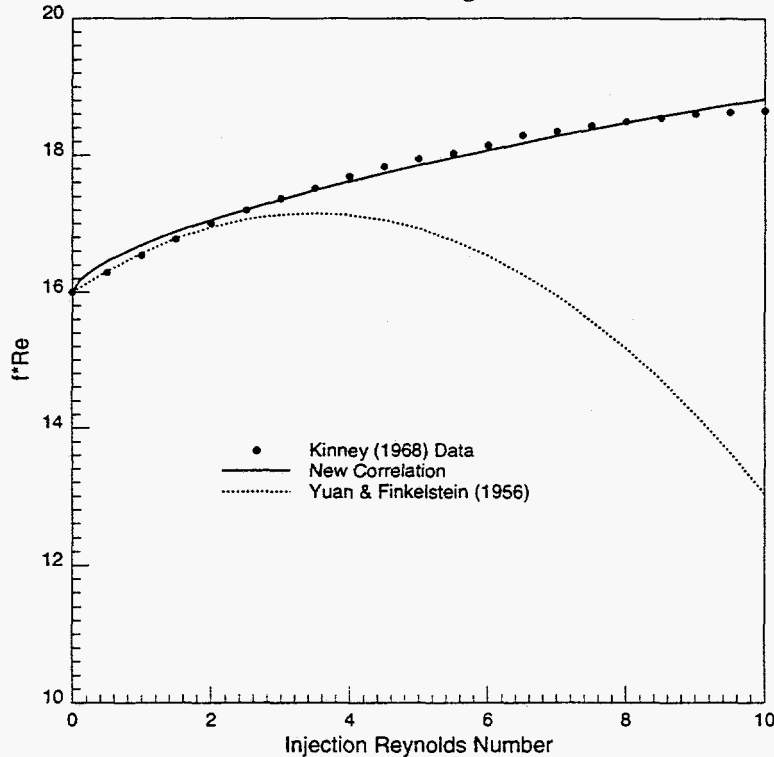
Figure 5.1: Effect of Inflow on Wall Friction Factor

Note that only a few experiments on laminar pipe flow with inflow or outflow have been reported in the literature.

5.2 Turbulent Flow in a Porous Pipe

A new correlation for the local wall friction factor for turbulent flow has also been developed in the present report by using Olson & Eckert's experimental data [16] for turbulent air flow in a porous pipe with uniform air injection through the pipe wall. The new correlation is:

$$f = f_0\left[1 - 29.03\left(\frac{R_{ew}}{R_e}\right)^{0.8003}\right] \tag{5.3}$$

Figure 5.2: Effect of Suction on Wall Friction Factor

As shown in Figure 5.3, the new correlation can provide satisfactory prediction of wall friction factor for porous pipe flow with injection through the pipe wall. The no-wall-flow friction factor f_0 can be determined either from the Colebrook-White [29, 30] equation or from one of its explicit approximations (Ouyang & Aziz, [26]).

For turbulent pipe flow with outflow (suction) through porous pipe wall, the local friction factor can be evaluated by the Kinney-Sparrow-Wallis's correlation [17]:
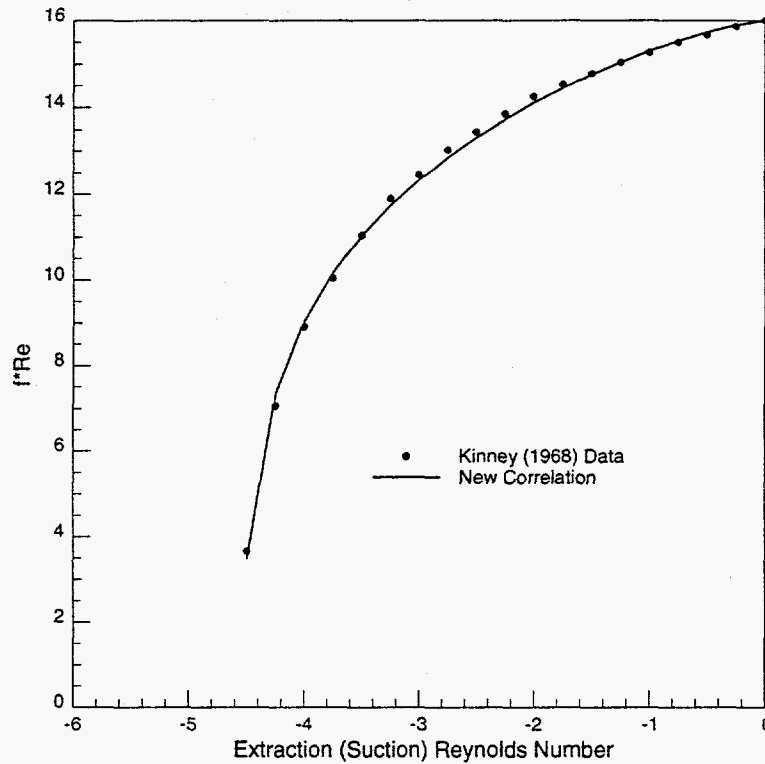
$$f = f_0 \left[1 - 17.5 \frac{R_{ew}}{R_e^{0.75}}\right] \tag{5.4}$$

5.3 Wellbore Flow

Both correlations (Eqs. 5.3 and 5.4) are based on experimental data for porous pipe flow. It is unclear whether they can also be used for normal wellbore flow conditions. We have applied Eq. 5.3 to analyse the single phase wellbore flow data from the 1995 stanford horizontal wellbore experiments [31] and found that it overpredicts the wall friction factor (Figure 5.4). Therefore, another new correlation for the local friction factor has been developed for wellbore turbulent flow based on the 1995 Stanford horizontal wellbore experiment data:

$$f = f_0 \left[1 - 0.0153 R_{ew}^{0.3978}\right] \tag{5.5}$$

As shown in Figure 5.4, Eq. 5.5 is a satisfactory correlation for local wall friction factor for single phase wellbore flow.
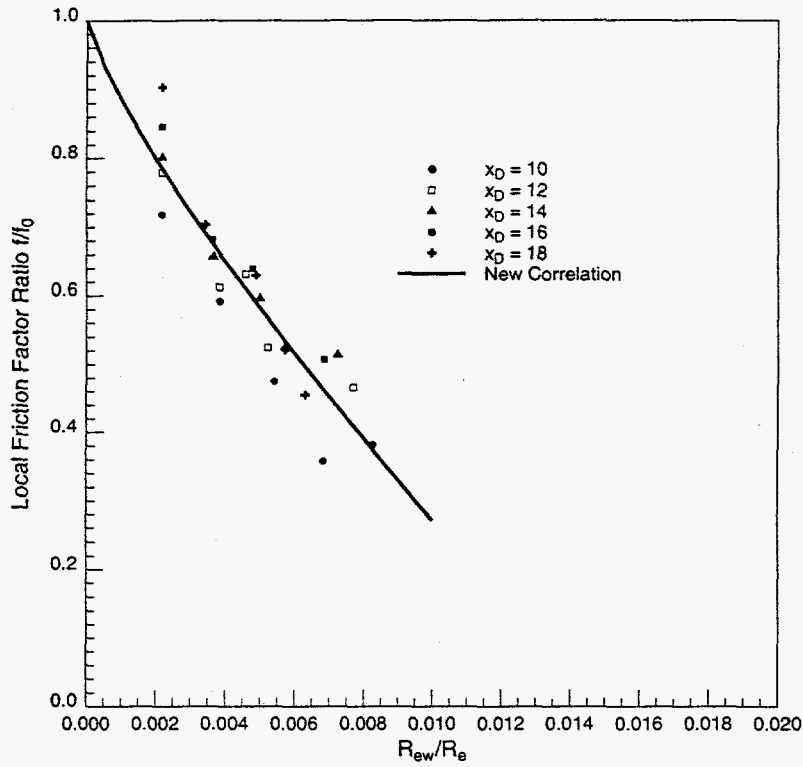
13

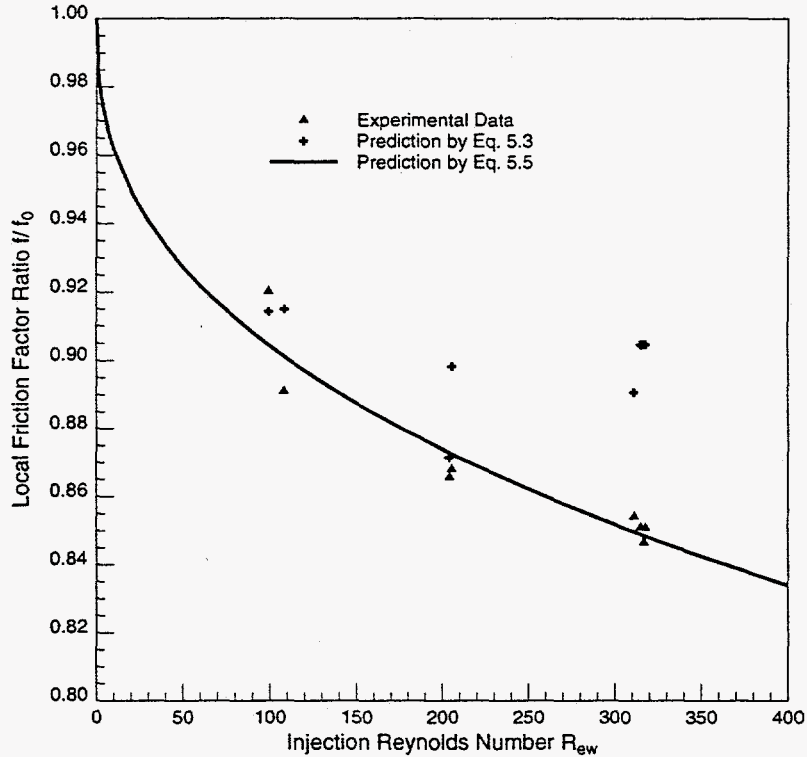Figure 5.3: Correlation of Wall Friction Factor for Turbulent Pipe Flow with Inflow

Figure 5.4: Correlation of Local Friction Factor for Turbulent Wellbore Flow

14

6. Results and Discussions

6.1 Accelerational to Frictional Pressure Gradient Ratio R_{af}

Figures 6.1, 6.2, and 6.3 show how the dimensionless number R_{af}, the accelerational to frictional pressure gradient ratio, changes with distance along the wellbore for uniform-influx horizontal wells with different wellbore lengths, production rates, and oil viscosities. These figures show that three regions exist along the wellbore, the laminar flow region, the partially-developed turbulent flow region, and the fully-developed turbulent flow region. The dimensionless number R_{af} is a constant in the laminar flow region that depends on fluid properties (viscosity and density), production rate and pipe geometry (pipe ID and pipe roughness). If all other parameters are fixed, then the shorter the horizontal well, or the higher the production rate, or the more viscous the oil, the larger the value of R_{af}, but the shorter the length of the laminar flow region. For the fully-developed turbulent flow region, all the R_{af} curves merge into one, which only changes with wellbore location. Between the laminar and the fully-developed turbulent flow region lies the partially-developed turbulent flow region where R_{af} varies with wellbore location, fluid properties, production rate and pipe geometry.
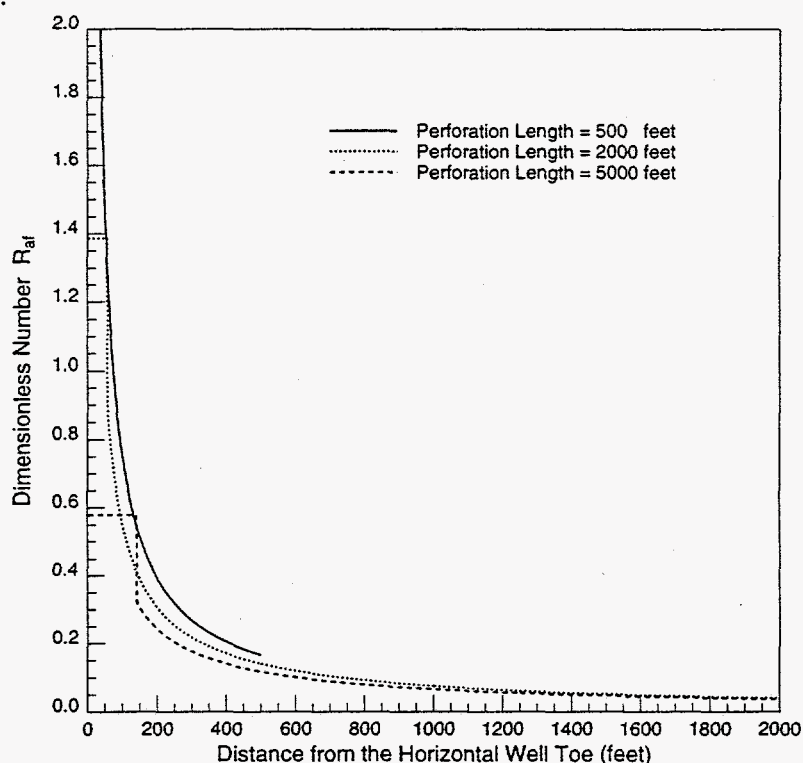

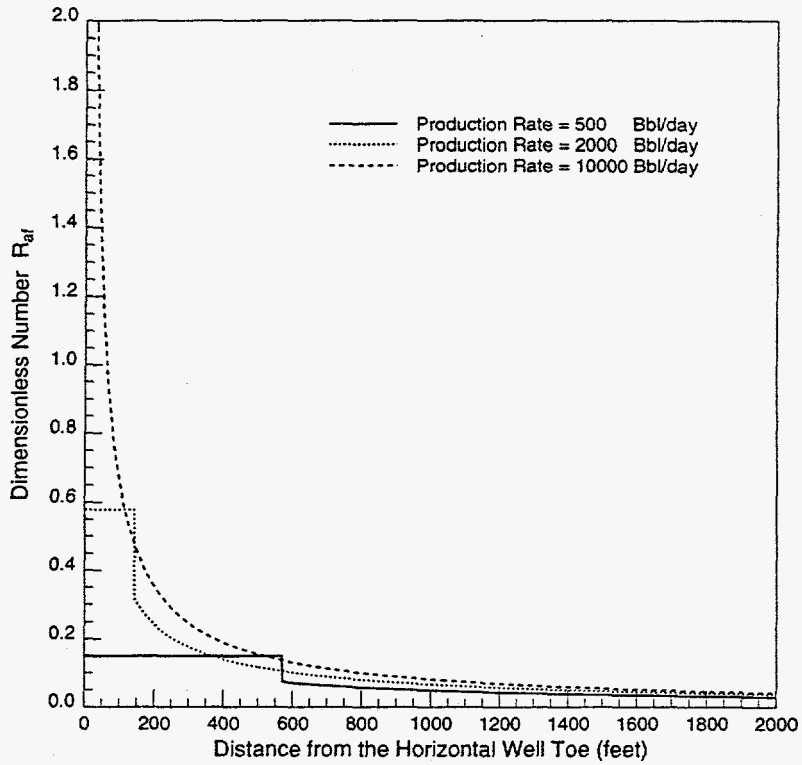Figure 6.1: Influence of Wellbore Length on R_{af}

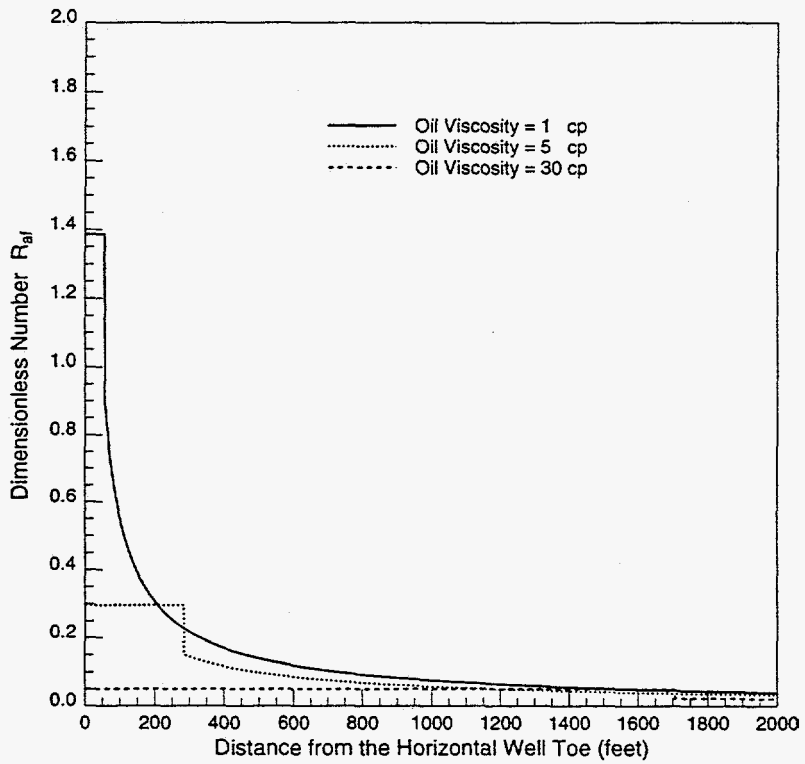Figure 6.2: Influence of Well Production Rate on R_{af}

Figure 6.3: Influence of Oil Viscosity on R_{af}

6.2 Analysis of the 1995 Stanford Horizontal Well Experimental Data

The new wellbore model has been applied to analyse single phase data from the 1995 Stanford Horizontal Wellbore Experiments. Figures 6.4 and 6.5 show variations of different friction factors and pressure drops over each 10 feet section with wellbore location for series IA2-6 experiments (Ouyang et al., [32]). Three friction factors are considered, the total or apparent friction factor f_T obtained on the basis of measured pressure drop, the actual friction factor f obtained from measurements by using the new wellbore flow model (to remove the accelerational and inflow-directional components from the total pressure drop), and the no-wall-flow friction factor f_0 obtained from the Colebrook-White equation [29, 30] by using local Reynolds number and effective pipe roughness. Figure 6.4 indicates that the apparent friction factor is larger than the no-wall-flow friction factor, while the actual friction is smaller than the no-wall-flow friction factor. The apparent friction factor is augmented by the inflow-induced accelerational pressure drop, and the actual friction factor is reduced (not increased) by inflow. This observation is consistent with our analysis of inflow influence mechanisms discussed in Section 4 and Appendix B. Frictional, accelerational as well as total pressure drops along every 10 feet section are shown in Figure 6.5. It is easy to see that the accelerational pressure drop is quite large and is as important as the frictional component. Therefore, negligence of the accelerational pressure drop will lead to errors and even incorrect conclusions. For example, if the accelerational pressure drop is not included, then the wall friction factor thus obtained is the apparent friction factor as shown in the Figure 6.4, which is larger than the no-wall-flow friction factor. This is contradictory to both theoretical analyses and experimental observations.

Similar conclusions are achieved for other experimental series, such as series IA3-A5 (Figures 6.6 and 6.7).

6.3 Partially-Perforated Horizontal Well Example

As shown in Figure 6.8, the partially-perforated horizontal well is refered to a well where only part of the wellbore is perforated to allow inflow. Also, it is assumed that the wellbore flow rate before the perforated zone, Q_0, may or may not be zero.

Figures 6.9 and 6.10 show pressure gradients and cumulative pressure drops from the start of the perforation in a partially-perforated horizontal well (well #1, see Table 6.1). Also shown in Figure 6.9 is the frictional pressure gradient determined from the no-wall-flow friction factor f_0. It is found that there is a nontrivial difference between the actual frictional pressure gradient and the frictional pressure gradient obtained from the no-wall-flow friction factor. The accelerational pressure gradient is comparable to the frictional component, and the dimensionless number R_{af} changes from 1.27 at the starting point of the well perforation to 0.71 at the end of the perforation. The cumulative accelerational pressure drop from the start point of the perforation is more or less the same as the cumulative frictional pressure drop (Figure 6.10).

17

Figure 6.4: Comparison of Different Friction Factors (Experimental Series IA2-6)

Figure 6.5: Comparison of Different Pressure Drop Components (Experimental Series IA2-6)
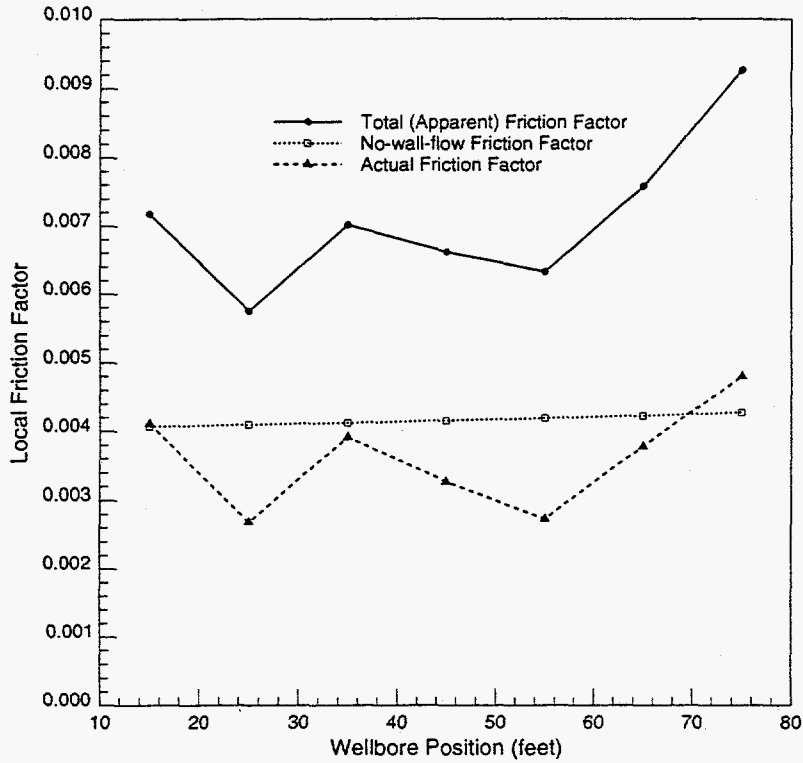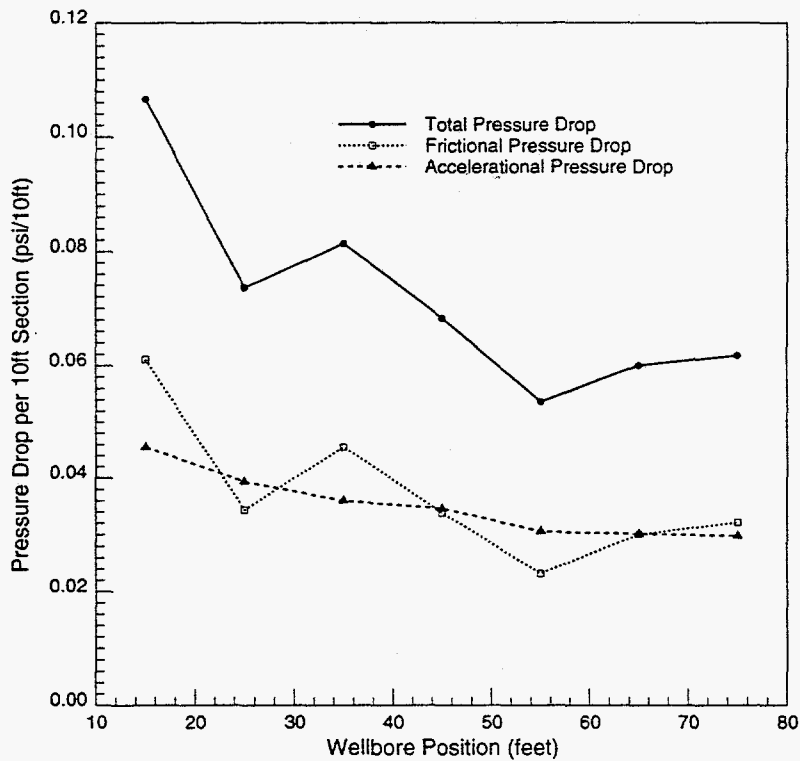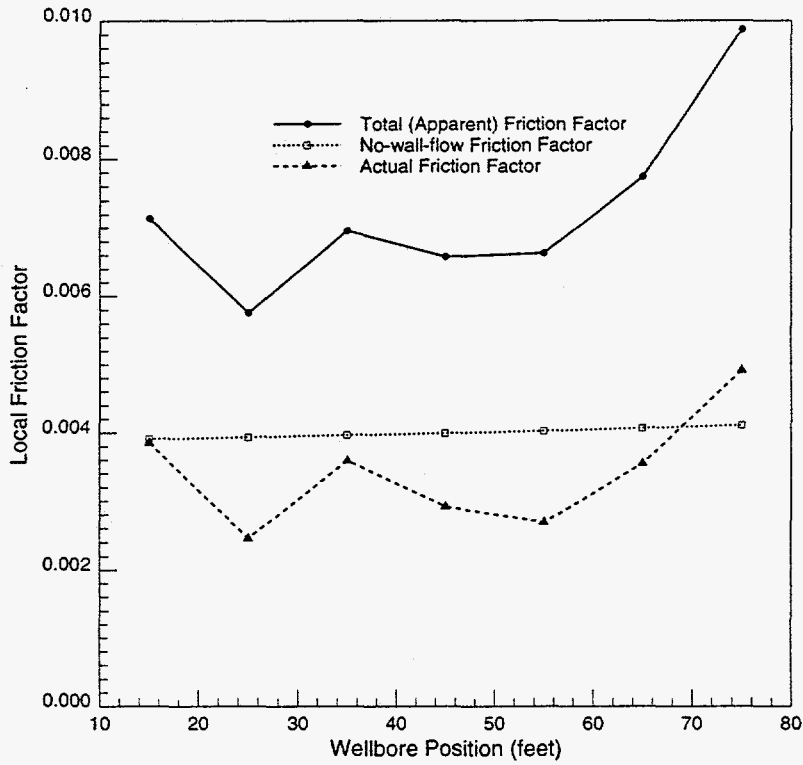
Figure 6.6: Comparison of Different Friction Factors (Experimental Series IA3-A5)
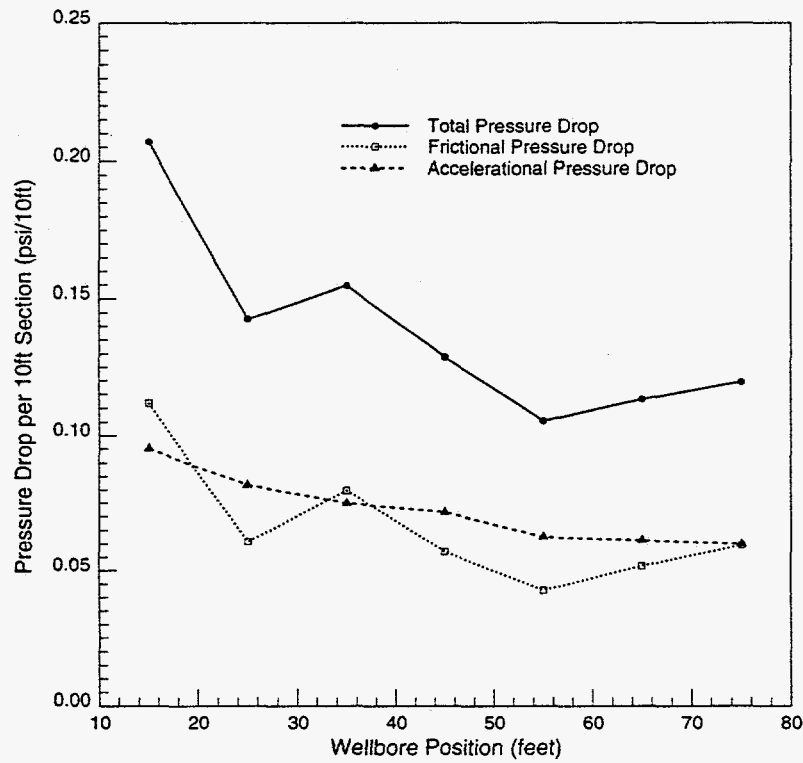

Figure 6.7: Comparison of Different Pressure Drop Components (Experimental Series IA3-A5)

Figure 6.8: Partially-Perforated Horizontal Wells

Figure 6.9: Pressure Gradients Change with Wellbore Location (well #1)

Figure 6.10: Change in Cumulative Pressure Drops with Wellbore Location (well #1)

6.4   Fully-Perforated Horizontal Well Example

In contrast to partially-perforated horizontal wells, fully-perforated horizontal wells have perforations over the entire wellbore length (Figure 6.11).

Figure 6.12 shows the change in pressure gradients with wellbore location for horizontal well #2 (see Table 6.1). In this case, the dimensionless pressure gradient ratio R_{af} ranges from 0.8 to 0.05, and the cumulative accelerational pressure drop is only about 6% of the total pressure drop along the whole wellbore, hence the accelerational pressure gradient is quite small compared to the frictional component for this horizontal well and only minor errors will result if the accelerational pressure drop is neglected.

6.5   Coupling the New Wellbore Model with a Reservoir Inflow Model

It is assumed in the above discussion that the specific inflow rate (i. e. the inflow rate per wellbore length) is the same everywhere along the whole wellbore. This is not necessarily true in a real horizontal well, since the wellbore pressure near the well toe is higher than that at the well heel due to wellbore pressure drop, the pressure drawdown near the well toe is less than that near the well heel, therefore, the specific inflow rate near the well toe should be smaller than that near the well heel. On the one hand, wellbore pressure or pressure drop is needed to determine the specific inflow rate distribution along the wellbore. On the other hand, the specific inflow rate distribution is an indispensable parameter to calculate wellbore pressure or pressure drop. Hence, a model which incorporates both the wellbore fluid flow and the fluid flow from reservoir into wellbore is required for determining specific
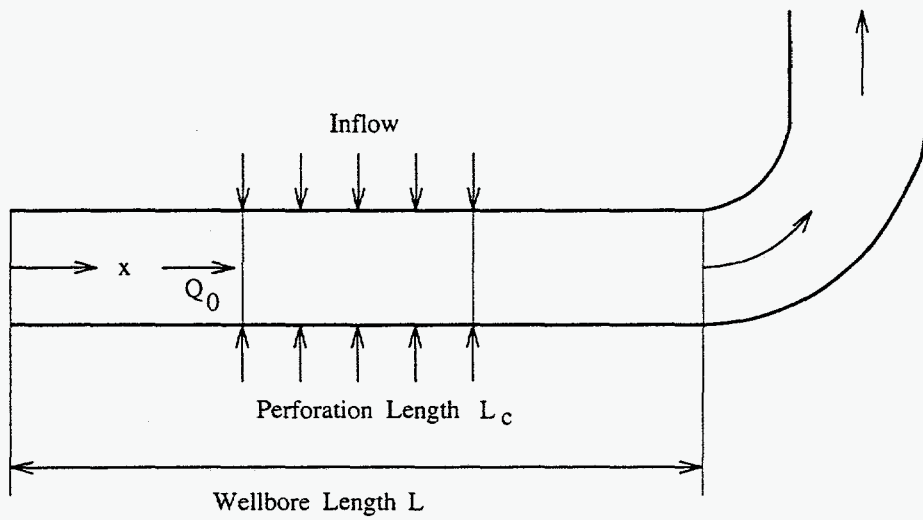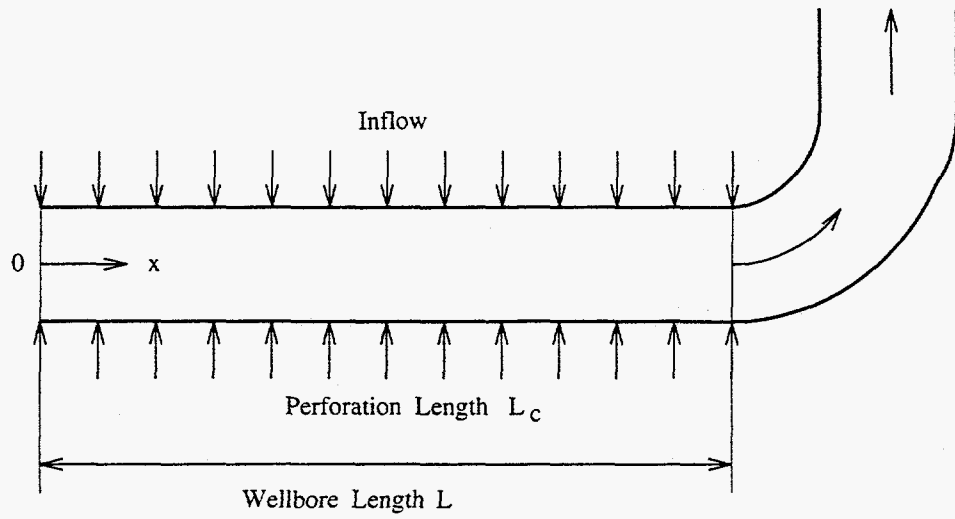
Figure 6.11: Fully-Perforated Horizontal Wells
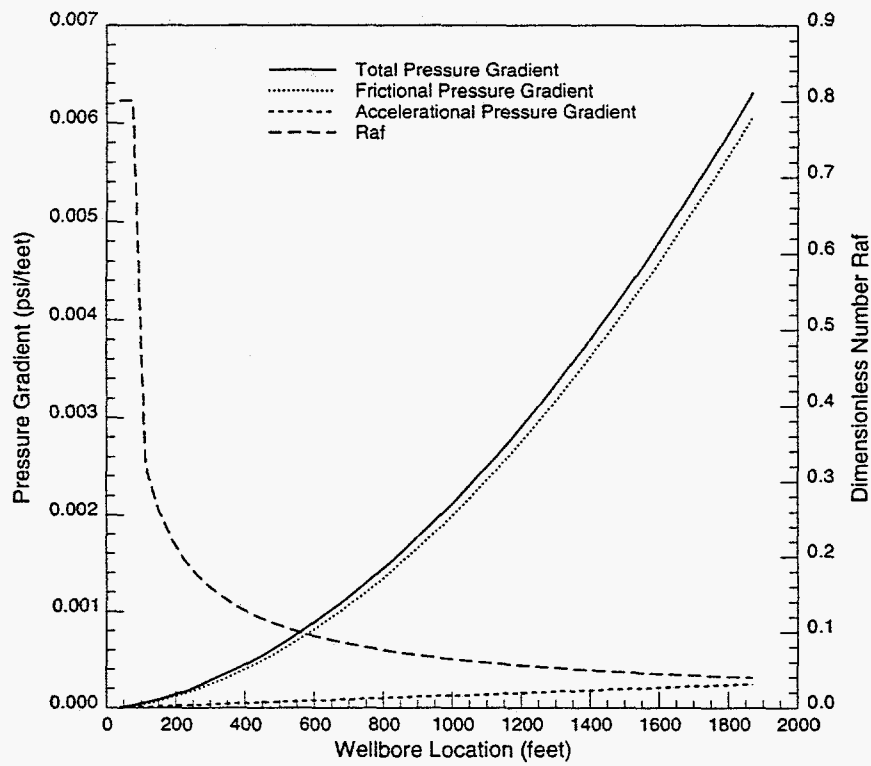
Figure 6.12: Pressure Gradients Change with Wellbore Location (well #2)

Table 6.1: Horizontal Well Parameters

Parameter	Well #1	Well #2	Well #3
Wellbore Length ($feet$)	100	1870	1000
Perforated Interval ($feet$)	100	1870	1000
Pipe ID ($inch$)	6.18	4.5	6
Relative Pipe Roughness	2.0×10^{-4}	1.0×10^{-4}	2.0×10^{-4}
Perforation ID ($inch$)	0.18	0.18	0.18
Perforation Density ($\frac{hole}{feet}$)	8	10	10
Inflow Direction (deg)	90	45	45
Fluid Density ($\frac{lbm}{ft^3}$)	62.4	52.44	62.0
Fluid Viscosity (cp)	0.878	2.5	1.0
Wellbore Rate before Completion Point ($\frac{Bbl}{day}$)	7000	N/A	N/A
Inflow Rate ($\frac{Bbl}{day}$)	7000	7500	N/A
Specific Inflow Rate ($\frac{Bbl}{day \times feet}$)	N/A	N/A	2.0

inflow rate distribution, wellbore pressure drop, and overall well production rate.

Since the reservoir inflow model is not the main issue of this report, a simple reservoir model as used by Dikken [1] and Novy [9] is applied to describe the reservoir fluid flow:

$$q_e(x) = J_s \left[p_e - p_w(x) \right] \tag{6.1}$$

As discussed in Section 3, the total pressure gradient for horizontal wells consists of three components, frictional, accelerational and inflow-directional. For the horizontal well #3 (Table 6.1), the frictional component contributes the largest part of the total pressure gradient, the accelerational component contributes in the range of 20% to 80% depending on the wellbore location (R_{af} changes from about 7.0 to 0.25), while the inflow-directional component contributes very little and can be neglected (Figure 6.13). Correspondingly the cumulative pressure drop along the wellbore is primarily caused by wall friction (which is also affected by inflow), while acceleration or kinetic energy changes only contribute about 5% to 10% to the overall pressure drop (Figure 6.14).

Specific inflow rate is not constant along the wellbore due to wellbore pressure drop (Figure 6.15). Significant differences occur between the real specific inflow rate predicted by considering pressure drop along the wellbore and the fictitious specific inflow rate where no pressure drop along the wellbore is assumed. For more accurate prediction of the specific inflow rate distribution, accelerational pressure drop should also be included in the wellbore model, otherwise around 10% overestimation of the specific inflow rate is likely to occur.

The well production rate is proportional to wellbore length if no pressure drop occurs along wellbore. The statement is invalid for many real horizontal wells. Figure 6.16 shows the production rate change with wellbore length. Well production rate decreases significantly due to pressure drop in the wellbore, and is likely to reach a maximum value at certain wellbore length beyond which no additional production is expected, no matter how long the horizontal well is. The well production rate decreases further if both frictional and accelerational pressure drops are included.
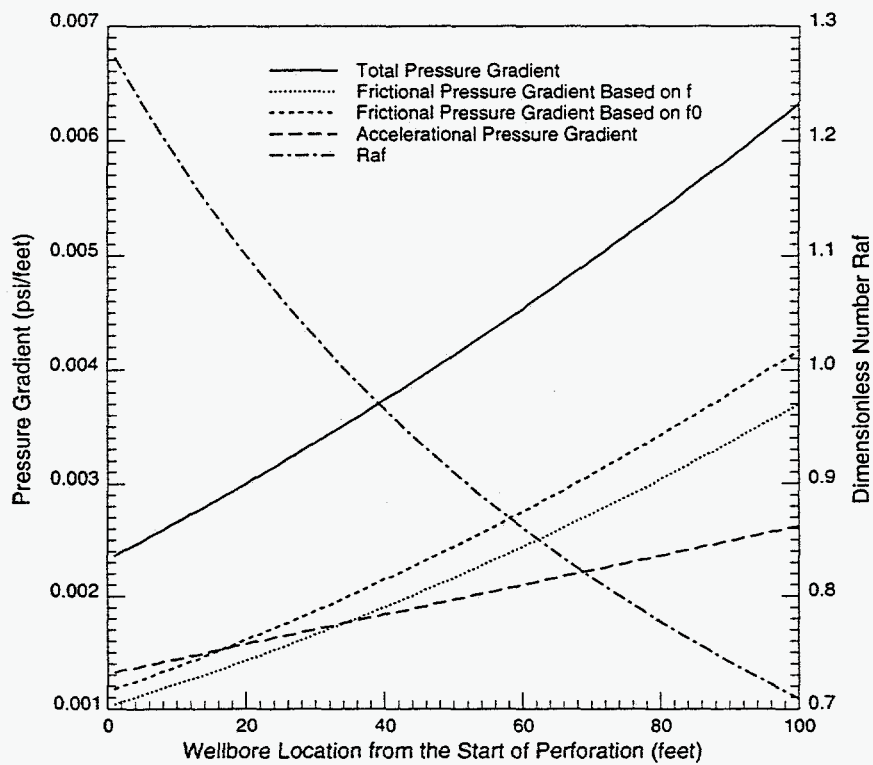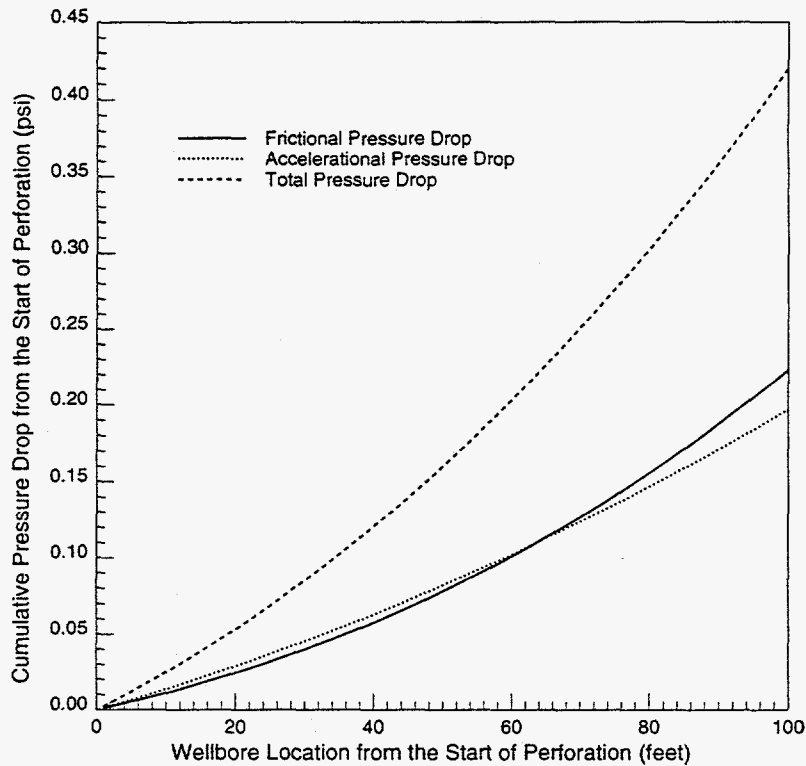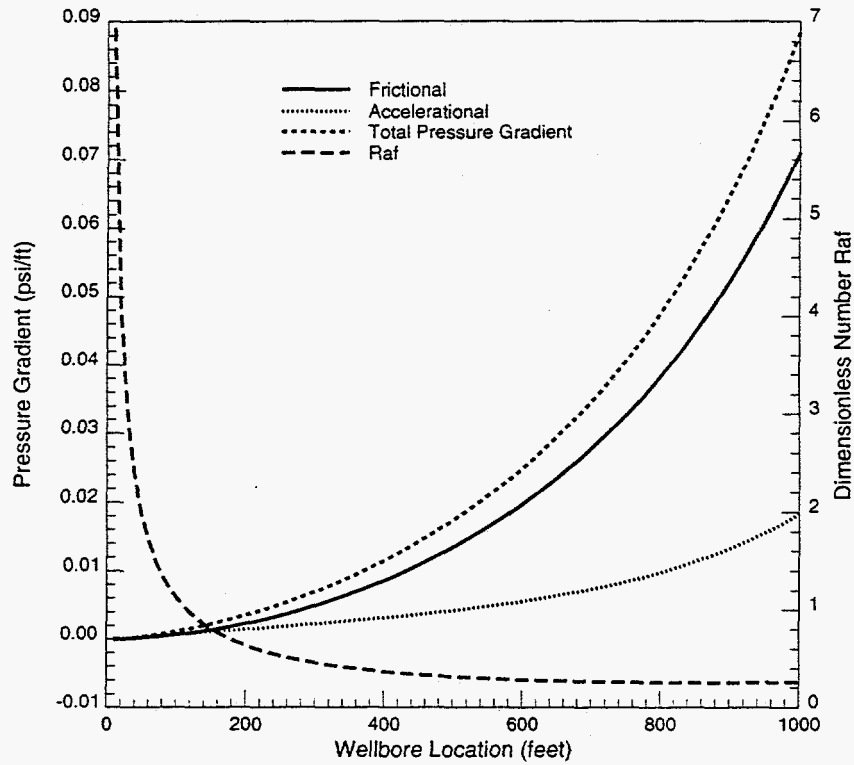
23

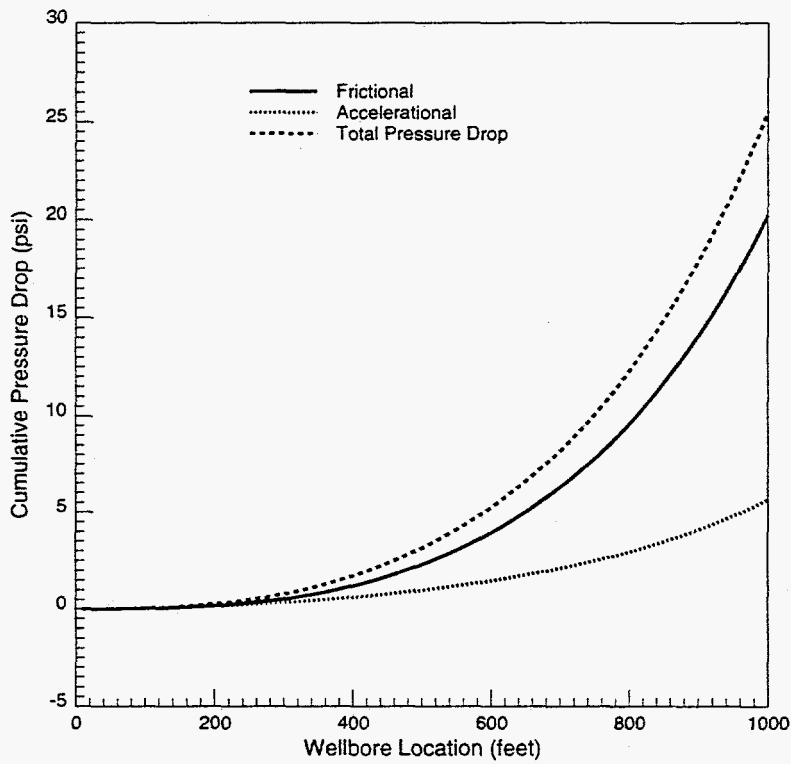Figure 6.13: Pressure Gradients Change with Wellbore Location (well #3)

Figure 6.14: Change in Cumulative Pressure Drops with Wellbore Location (well #3)

24
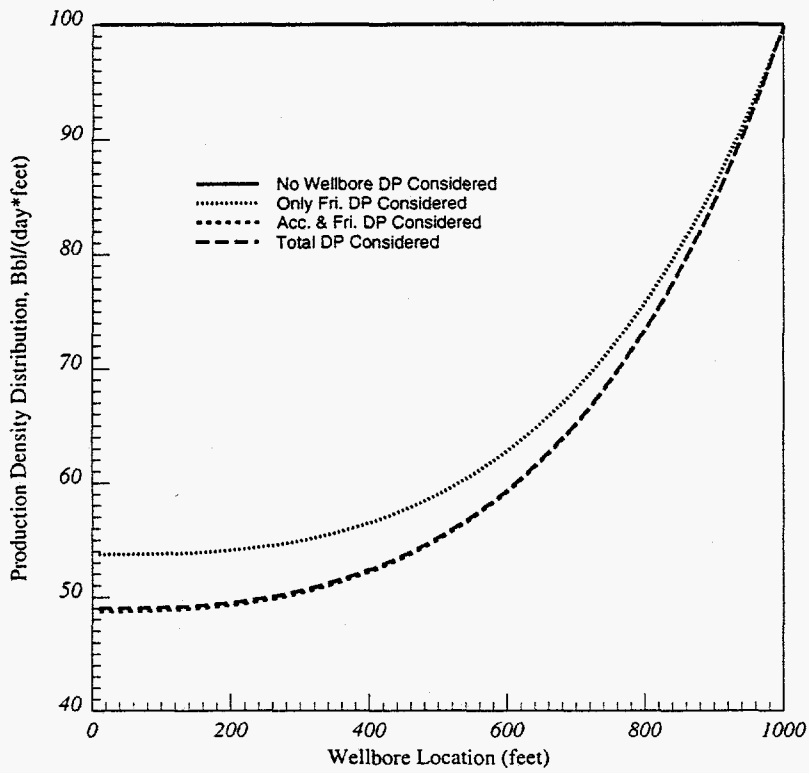
Figure 6.15: Specific Inflow Rate Distribution (well #3)
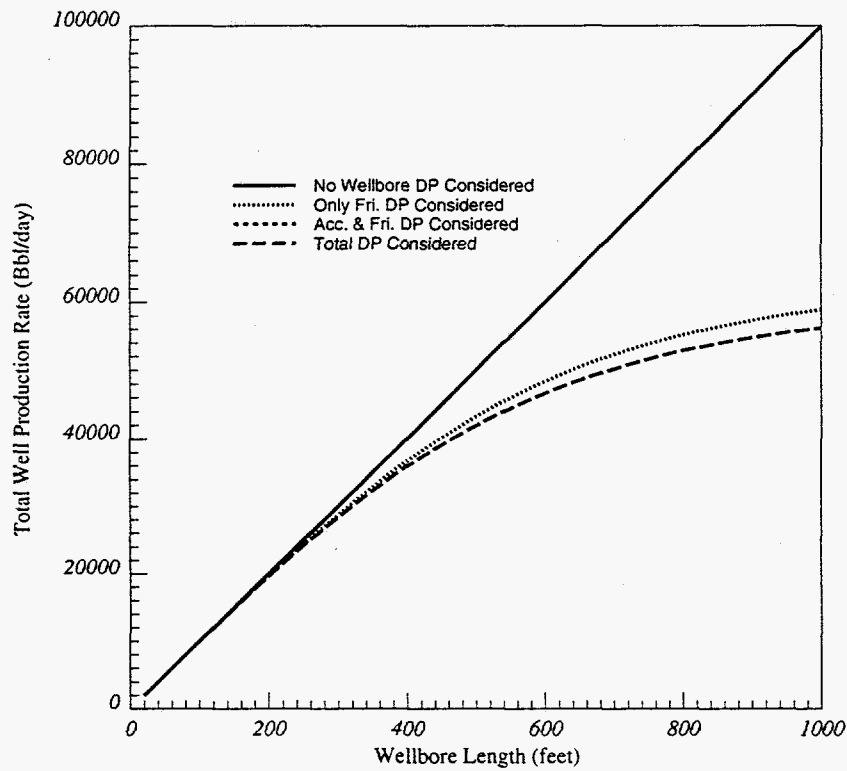
Figure 6.16: Overall Well Production Rate Change with Wellbore Length (well #3)

7. Conclusions

A general single phase wellbore flow model, which incorporates not only frictional, accelerational and gravitational pressure drops, but also the pressure drop caused by inflow, is presented in this report. The new wellbore model is readily applicable to any wellbore perforation patterns and well completions, and can be easily incorporated in reservoir simulators or analytical reservoir inflow models.

Inflow and outflow affect wall friction shear. The influence of either inflow or outflow depends on the flow regime present in the wellbore. Inflow (production wells) increases the wall friction for laminar flow while decreases the friction for turbulent flow. The opposite is true for outflow (injection wells).

New wall friction factor correlations for pipe flow with influx have been developed based on the published research work and the Stanford horizontal wellbore experimental data. They can be applied for wellbore flow to determine wall friction shear and thus frictional pressure drop for either inflow (production well) or outflow (injection well) and for either laminar flow or turbulent flow.

It is shown that accelerational pressure drop may or may not be important compared to the frictional component depending on the specific pipe geometry, fluid properties and flow conditions.

Nomenclature

A pipe cross-section area
D pipe internal diameter (ID)
D_I perforation internal diameter
f Fanning friction factor
f_0 no-wall-flow Fanning friction factor
f_T total or apparent Fanning friction factor
g acceleration due to gravity
g_c conversion factor
L wellbore length
L_t wellbore length for laminar flow region
m velocity profile index
n perforation density
p pressure
q_e specific inflow rate
q_w local wellbore flow rate
r radial coordinate
R_{af} ratio between accelerational and frictional pressure gradient
R_{gf} ratio between gravitational and frictional pressure gradient
R_{da} ratio between inflow-directional and accelerational pressure gradient
R_e Reynolds number
R_{et} transition Reynolds number from laminar to turbulent flow
R_{eft} transition Reynolds number to fully-developed turbulent flow

26

R_{ew} wall Reynolds number, positive for injection and negative for suction

S wellbore perimeter

u axial velocity

u_{max} maximum velocity in velocity profile

u_τ friction velocity for turbulent flow

u^+ normalized velocity for turbulent flow

U average axial velocity

U_n average velocity for no inflow or outflow case

U_w average velocity for inflow or outflow case

U_∞ free stream velocity

V volume

V_w wall inflow or outflow velocity

x axial coordinate

y local counter-radial coordinate

y_1 thickness of the viscous sublayer

y_2 thickness of the buffer sublayer

Greek Letters

α momentum correction factor

γ inflow direction angle

δ boundary layer thickness

θ wellbore inclination angle

μ fluid viscosity

ν kinetic fluid viscosity

ρ fluid density

τ_w wall friction shear stress

Subscripts

acc   accelerational

ele   elevational or gravitational

fri   frictional

tur   turbulent

vis   viscous

27

References

[1] B. J. Dikken. "Pressure Drop in Horizontal Wells and its Effect on Production Performance". *J of Petroleum Technology*, 42(11):1426–1433, 1990.

[2] M. R. Islam and A. Chakma. "Comprehensive Physical and Numerical Modelling of a Horizontal Well". In *The 65th SPE Annual Technical Conference and Exhibition*, New Orleans, LA, 1990. paper SPE 20627.

[3] A. N. Folefac, J. S. Archer, R. I. Issa, and A. M. Arshad. "Effect of Pressure along Horizontal Wellbore on Well Performance". In *The Offshore Europe Conference*, Aberdeen, 1991. paper SPE 23094.

[4] P. Briggs. "Pressure Drop in Horizontal Well Completions—Is It Important?". In *1991 JETEC conference*, 1991.

[5] E. Ozkan, C. Sarica, and M. Haciislamoglu. "Effect of Conductivity on Horizontal Well Pressure Behavior ". In *The 67th SPE Annual Technical Conference and Exhibition*, Washington, D. C., 1992. paper SPE 24683.

[6] M. Ihara and N. Shimizu. "Effect of Accelerational Pressure Drop in a Horizontal Wellbore ". In *The 68th SPE Annual Technical Conference and Exhibition*, Houston, Texas, 1993. paper SPE 26519.

[7] K. Seines, I. Aavatsmark, S. C. Lien, and P. Rushworth. "Considering Wellbore Friction Effects in Planning Horizontal Wells". *J of Petroleum Technology*, 45(10):994–1000, 1993.

[8] M. J. Landman. "Analytic Modelling of Selectivity Perforated Horizontal Wells". *J of Petroleum Science and Engineering*, 10:179–188, 1994.

[9] R. A. Novy. "Pressure Drops in Horizontal Wells: When Can They Be Ignored?". *SPE Reservoir Engineering*, 10(1):29–35, 1995.

[10] H. Schlichting. *"Boundary-Layer Theory"*. McGraw-Hill Book Co., New York, 7 edition, 1987. translated by Kestin J.

[11] M. R. Wiesner and S. J. Chellam. "Mass Transfer Considerations for Pressure-Driven Membrane Processes". *American Water Works Association J.*, 84(1):88–95, 1992.

[12] J. P. Hartnett. "Mass Transfer Cooling ". In *Handbook of Heat and Transfer Applications, 2nd Edition (edited by W. M. Rohsenow et al.)*, McGraw-Hill Book Co., New York, 1985.

[13] A. S. Berman. "Effects of Porous Boundaries on the Flow of Fluids in Systems of Various Geometries". In *2nd U. N. Conference on the Peaceful Uses of Atomic Energy*, Geneva, Sept 1–13, 1958. vol 4, 351–358.

[14] S. W. Yuan and A. B. Finkelstein. "Laminar Pipe Flow with Injection and Suction through a Porous Wall". *Trans ASME*, 78:719–724, 1956.

[15] R. B. Kinney. "Fully Developed Frictional and Heat-transfer Characteristics of Laminar Flow in Porous Tubes". *Int J Heat Mass Transfer*, 11:1393–1400, 1968.

[16] R. M. Olson and E. R. G. Eckert. "Experimental Studies of Turbulent Flow in a Porous Circular Tube with Uniform Fluid Injection through the Tube Wall". *J of Applied Mechanics*, 33(1):7–17, 1966.

[17] R. B. Kinney and E. M. Sparrow. "Turbulent Flow, Heat Transfer and Mass Transfer in a Tube with Surface Suction". *J Heat Transfer*, 92:117–125, 1970.

[18] L. Merkine, A. Solan, and Y. Winograd. "Turbulent Flow in a Tube with Wall Suction". *J Heat Transfer*, 93:242–244, 1971.

[19] H. L. Weissberg and A. S. Berman. "Velocity and Pressure Distribution in Turbulent Pipe Flow with Uniform Suction". In *Proc Heat Transfer Fluid Mechanics Inst.*, 1955. 1–30.

[20] M. R. Doshi and W. N. Gill. "Turbulent Flow in a Tube with Wall Suction". *J. Heat Transfer*, 96:251–252, 1974.

[21] G. Lombardi, E. M. Sparrow, and E. R. G. Eckert. "Experiments on Heat Transfer to Transpired Turbulent Pipe Flows". *Int J. Heat Mass Transfer*, 17:429–437, 1974.

[22] G. Raithby. "Laminar Heat Transfer in the Thermal Entrance Region of Circular Tubes and Two-Dimensional Rectangular Ducts with Wall Suction and Injection". *Int. J. Heat and Mass Transfer*, 14(1):223–243, 1971.

[23] J. Kloster. "Experimental Research on Flow Resistence in Perforated Pipe ". Master's thesis, Norwegian Institute of Technology, 1990.

[24] H. Asheim, J. Kolnes, and P. A. Oudeman. "Flow Resistance Correlation for Completed Wellbore". *J of Petroleum Science and Engineering*, 8:97–104, 1992.

[25] M. Ihara, K. Kikuyama, Y. Hasegawa, and K.Mizuguchi. "Flow in Horizontal Wellbores with Influx through Porous Walls ". In *The 69th SPE Annual Technical Conference and Exhibition*, New Orleans, LA, 1994. SPE 28485.

[26] L-B Ouyang and K. Aziz. "Steady-State Gas Flow in Pipes". *J of Petroleum Science and Engineering*, 14:137–158, 1996.

[27] P. E. Gill, W. Murray, and W. H. Wright. *"Practical Optimization"*. Academic Press, London, UK, 1981. 401pp.

[28] L-B Ouyang. "Stratified Flow Model and Interfacial Friction Factor Correlations". Master's thesis, Stanford University, Stanford, California, June 1995.

[29] C. F. Colebrook and C. M. White. "Experiments with Fluid Friction in Roughened Pipes". *Proc. Roy Soc. (London)*, 161A:367–381, 1937.

[30] C. F. Colebrook. "Turbulent Flow in Pipes, with Particular Reference to the Transition Region between the Smooth and Rough Pipe Laws". *J. Instn. Civil Engrs. (London)*, 12:133–156, 1939.

[31] L-B Ouyang, S. Arbabi, and K. Aziz. "General Wellbore Flow Model for Horizontal, Vertical and Slanted Well Completions". In *The 71st Annual SPE Technical Conference & Exhibition*, Denver, Colorado, 1996. paper SPE 36608.

[32] L-B Ouyang, S. Arbabi, and K. Aziz. "Preliminary Analysis of the 1995 Stanford Horizontal Wellbore Experiments". In *Productivity and Injectivity of Horizontal Wells*, Stanford University, 1996. Annual Technical Report for DOE, 1–24.

[33] F. M. White. *"Fluid Mechanics"*. McGraw–Hill Book Co., New York, NY, 1986.

[34] K. Aziz. "Ways to Calculate Gas Flow and Static Head". *Petroleum Engineer*, 34–35, 1962–1963. series articles.

[35] H. L. Weissberg. "Laminar Flow in the Entrance Region of a Porous Pipe". *The Physics of Fluids*, 2(5):510–516, 1959.

[36] R. W. Hornbeck, W. T. Rouleau, and F. Osterle. "Laminar Entry Problem in Porous Tubes". *The Physics of Fluids*, 6(11):1649–1654, 1963.

[37] M. Fredman and J. Gillis. "Viscous Flow in a Pipe with Absorbing Walls". *J. Applied Mechanics*, 34:819–822, 1967.

[38] R. C. Gupta. "Laminar Flow in the Inlet Region of a Porous Tube". *Applied Science Research*, 22:360–365, 1970.

[39] J. P. Quaile and E. K. Levy. "Laminar Flow in a Porous Tube with Wall Suction". *J Heat Transfer*, 97:66–71, 1975.

[40] A. J. Ward-Smith. *"Internal Fluid Flow"*. Clarendon Press, Oxford, England, 1980. 566pp.

Appendix A. Derivation of General Wellbore Flow Model

A.1 Model Development

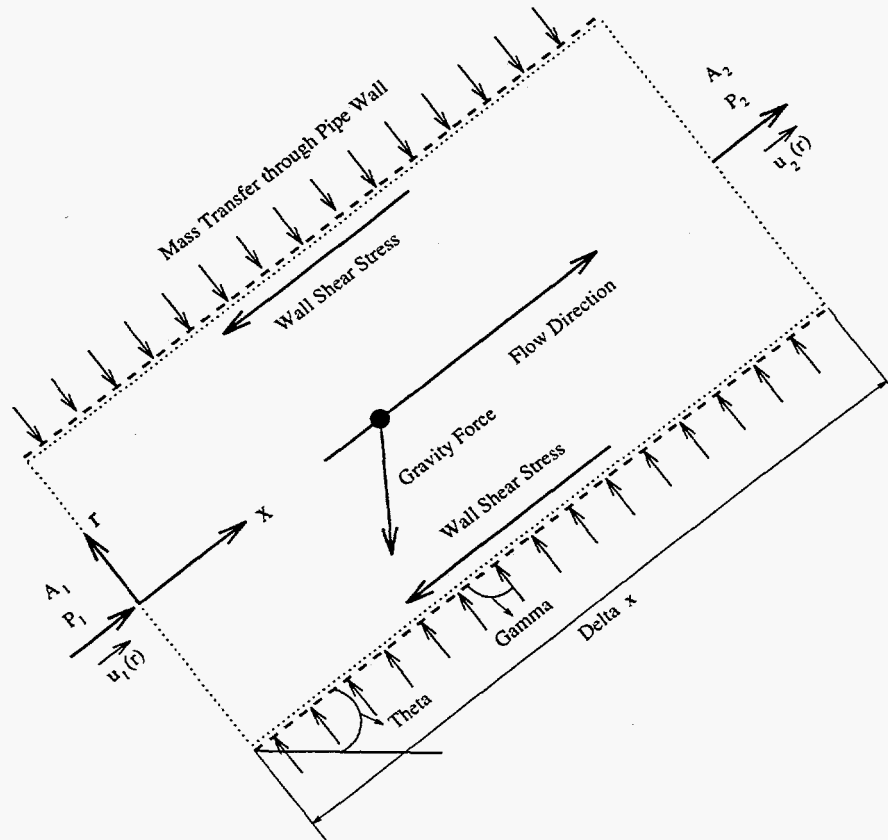Consider fluid flow in a wellbore as shown in Figure A.1 and assume:

Figure A.1: Mass and Momentum Transfer along a Wellbore with Mass Transfer through Perforations

- single phase flow;

- incompressible Newtonian fluid;

- isothermal flow;

- no heat transfer to and from the fluid to the environment;

- no mechanical work done on or by the fluid during its passage through the pipe (No shaft work or work of compression).

With these assumptions, the momentum balance equation takes the form

$$\sum \vec{F} = \frac{\partial}{\partial t} \iiint_{CV} \rho \vec{u} dV + \iint_{CS} \rho \vec{u} (\vec{u} \cdot \vec{n}) dA \tag{A.1}$$

where CV represents the "control volume" and CS "control surface" or "control area".

For steady-state pipe flows

$$\frac{\partial}{\partial t} \iiint_{CV} \rho \vec{u} dV = 0 \tag{A.2}$$

Average velocities over cross-sections are usually employed to reduce a two-dimensional problem to a one-dimensional problem. This is the most convenient approximation to make the problem tractable. Although the axial velocity is nonuniform over the whole pipe cross-section, $\vec{u} = \vec{u}(x, r)$, it can be approximated by an average value U by introducing the momentum correction factor α

$$\iint_A \rho u (\vec{u} \cdot \vec{n}) dA = \frac{1}{\alpha} \rho A U^2 \vec{n} \tag{A.3}$$

where the correction factor α is used to compensate for the variation of fluid velocity over the pipe cross-section. The value of α depends on the velocity profile and is 0.75 for fully-developed laminar flow while it ranges from 0.9643 to about 0.9895 for fully-developed turbulent flow (White, [33]; Ouyang & Aziz, [26]). Aziz [34] suggested that a value of 0.9 be used for practical gas flow problems.

Using the average velocity and momentum correction factor, Eq. A.1 can be expanded as

$$
\begin{aligned}
\left[(pA)_2 - (pA)_1 \right] &= \left[\frac{1}{\alpha_1 g_c} \rho A_1 U_1^2 - \frac{1}{\alpha_2 g_c} \rho A_2 U_2^2 \right] \\
&\quad + \frac{n \triangle x}{\alpha_I g_c} \rho A_I U_r U_x - \tau_w S \triangle x \\
&\quad - \rho \bar{A} \triangle x \frac{g}{g_c} \sin \theta
\end{aligned} \tag{A.4}
$$

where

- The LHS term is the net pressure force acting on the control volume;

- The first term in the RHS is the net momentum increase caused by axial flow velocity change due to inflow and fluid compression or expansion;

- The second term in the RHS is the net momentum increase introduced by inflow directional effects;

- The third term in the RHS is the shear stress acting on the pipe wall, where the area $S \triangle x$ should be replaced by $S \triangle x - A_I n \triangle x$ if the actual shear stress acting area is to be considered;

- The fourth term in the RHS is the gravitational force contribution.

Mass balance equation

$$\rho U_1 A_1 + n \triangle x \rho A_I U_I = \rho U_2 A_2 \tag{A.5}$$

where n is the hole or perforation density (the number of holes or shots per unit pipe length).

Single phase fluid flow is assumed, i.e., the fluid in the axial direction is the same as that coming through perforations. Whenever the axial flow is different from the perforation flow, two-phase or multiphase models should be applied. Examples of two-phase flow in a horizontal well include air inflow with water axial flow, water axial flow with oil inflow, air/water axial flow with air inflow, etc.

Consider flow in a very tiny segment of the pipe, i. e. $\triangle x \to 0$, then it is reasonable to assume that $A_1 \approx A_2 \approx A$, thus Eq. A.5 becomes

$$U_2 = U_1 + n \triangle x \frac{A_I}{A} U_I \tag{A.6}$$

Substituting Eq. A.6 into Eq. A.4 and taking the limit $\triangle x \to 0$ lead to the following pressure gradient equation

$$
\begin{aligned}
\frac{dp}{dx} &= -\frac{\rho}{g_c} \frac{d}{dx} \left(\frac{U^2}{\alpha} \right) + \frac{n}{\alpha_I g_c} \rho \frac{A_I}{A} U_r U_x \\
&\quad - \tau_w \frac{S}{A} - \rho \frac{g}{g_c} \sin \theta
\end{aligned}
\tag{A.7}
$$

In Eq. A.7, the right hand side includes four different terms: the pressure gradient due to kinetic energy change (accelerational effects), the pressure gradient due to the inflow direction, the frictional pressure gradient, and the gravitational pressure gradient. Here two additional terms come into play due to inflow, compared to single phase pipe flow without inflow or outflow.

Since turbulent flow occurs along almost the whole wellbore section for most practical situations, the momentum correction factor α does not change much for different velocity profiles (Ouyang & Aziz, [26]), hence, α can be taken as constant. Besides, the derivative $\frac{dU}{dx}$ can be obtained from Eq. A.6

$$\frac{dU}{dx} = n \frac{A_I}{A} U_I \tag{A.8}$$

So, Eq. A.7 can be rearranged as

$$
\begin{aligned}
\frac{dp}{dx} &= -n \frac{A_I}{A} \frac{2\rho}{g_c \alpha} U U_I + n \frac{A_I}{A} \frac{\rho}{2 g_c \alpha_I} U_I^2 \sin 2\gamma \\
&\quad - \tau_w \frac{S}{A} - \rho \frac{g}{g_c} \sin \theta
\end{aligned}
\tag{A.9}
$$

where γ is the injection angle (Figure A.1), A_I the cross-section area of each perforation.

The equation for the wall friction shear can be obtained from Eq. A.9

$$\tau_w = \frac{D}{4} \left[\frac{dp}{dx} - n \frac{A_I}{A} \frac{2\rho}{g_c \alpha} U U_I + n \frac{A_I}{A} \frac{\rho}{2 g_c \alpha_I} U_I^2 \sin 2\gamma - \rho \frac{g}{g_c} \sin \theta \right] \tag{A.10}$$

33

Once the wall friction shear stress τ_w is computed, the wall friction factor can also be determined by

$$f = \tau_w / \left[\frac{1}{2g_c} \rho U^2 \right] \tag{A.11}$$

In most practical applications, the inflow direction is normal or nearly normal to the pipe wall, i. e. $\gamma = \frac{\pi}{2}$, so Eqs. A.9 and A.10 can be further simplified to

$$\frac{dp}{dx} = -n \frac{A_I}{A} \frac{2\rho}{g_c \alpha} U U_I - \tau_w \frac{S}{A} - \rho \frac{g}{g_c} \sin \theta \tag{A.12}$$

$$\tau_w = \frac{D}{4} \left[\frac{dp}{dx} - n \frac{A_I}{A} \frac{2\rho}{g_c \alpha} U U_I - \rho \frac{g}{g_c} \sin \theta \right] \tag{A.13}$$

A.2 Relative Importance of Different Pressure Gradient Components

Eq. A.9 implies that the total pressure gradient along a wellbore consists of four different components, accelerational, inflow-directional, frictional and gravitational. In order to quantitatively describe the relative importance of different pressure gradient components, three dimensionless numbers are defined:

$$R_{af} = \frac{\left(\frac{dp}{dx}\right)_{acc}}{\left(\frac{dp}{dx}\right)_{fri}} = \frac{q_e D}{\alpha f q_w} \tag{A.14}$$

$$R_{gf} = \frac{\left(\frac{dp}{dx}\right)_{ele}}{\left(\frac{dp}{dx}\right)_{fri}} = \frac{g D \sin \theta}{2 f U^2} \tag{A.15}$$

$$R_{da} = \frac{\left(\frac{dp}{dx}\right)_{dir}}{\left(\frac{dp}{dx}\right)_{acc}} = \frac{\alpha}{4\alpha_I} \frac{U_I}{U} \sin 2\gamma \tag{A.16}$$

With these definitions, the total pressure gradient takes the following simple form

$$\frac{dp}{dx} = -\frac{4\tau_w}{D} [1 + R_{af}(1 - R_{da}) + R_{gf}] \tag{A.17}$$

It is easily seen from Eq. A.14 that the closer we are to the horizontal well toe ($x = 0$), the smaller the local wellbore production rate q_w, thus the larger the R_{af} and the more important the accelerational pressure gradient. In contrast, near the heel of the horizontal well ($x = L$), the local production rate q_w becomes large and close to the total well production rate, while the specific influx (inflow rate per wellbore length) q_e does not change significantly, so R_{af} is small, and the accelerational pressure gradient is small and may be negligible.

For the uniform inflow case, Eq. A.14 and Eq. A.16 can be simplified

$$R_{af} = \frac{D}{\alpha f x} \tag{A.18}$$

34

$$R_{da} = \frac{\alpha}{4\alpha_I nx} \frac{A}{A_I} \sin 2\gamma \tag{A.19}$$

and the local axial Reynolds number can be computed by

$$R_e = R_e(x) = \frac{4\rho x q_e}{\pi \mu D} \tag{A.20}$$

As we know, laminar flow occurs below certain transition Reynolds number R_{et}. For pipe flow without mass injection or extraction through pipe wall, R_{et} can be taken as 2100. Based on the transition Reynolds number, we can determine the transition pipe location L_t, beyond which the flow is turbulent, i. e.

- If $x \leq L_t$, the flow is laminar;

- If $x > L_t$, the flow is turbulent.

The value of L_t is dependent on pipe ID, fluid properties (such as density and viscosity), and inflow rates. For the whole range of reservoir oil types,

$$\mu = 0.1 \; cp \; \sim \; 1000 \; cp$$

$$\rho = 40 \; lbm/ft^3 \; \sim \; 100 \; lbm/ft^3$$

correspondingly

$$L_t = [5.278 \times 10^{-7} \; \sim \; 1.319 \times 10^{-2}] \frac{DR_{et}}{q_e} \tag{A.21}$$

the higher the specific influx q_e, the smaller the laminar flow length, provided that the other parameters are fixed.

R_{af} behaves quite differently in different flow regimes

- Laminar flow $(x \leq L_t)$

$$R_{af} = \frac{\rho q_e}{4\pi \alpha \mu F(R_{ew})} \tag{A.22}$$

where the injection Reynolds number $R_{ew} = \frac{\rho q_e}{\pi \mu}$.

Therefore, R_{af} only depends on fluid properties, inflow rate and pipe ID, but it is independent of location x and pipe roughness ϵ. The larger the q_e, the larger the R_{af}, but the shorter the laminar flow length L_t.

- Turbulent flow $(x > L_t)$

  In this region,

$$f = f_0 \left(\frac{\epsilon}{D}, R_e \right) G \left(R_{ew}, R_e \right) \tag{A.23}$$

35

where $f_0(\frac{\epsilon}{D}, R_e)$ is the Fanning friction factor for pipe flow without inflow, and the function $G(R_{ew}, R_e)$ is introduced to account for the inflow effect and its form has been given in the Section 5 of this report.

The turbulent flow region can be divided further into two subregimes: the partially-developed turbulent flow (transition) and the fully-developed turbulent flow. In the partially-developed turbulent flow regime, the friction factor $f_0(\frac{\epsilon}{D}, R_e)$ is dependent on both the local Reynolds number and the relative pipe roughness, whereas in the fully-developed turbulent flow regime, the friction factor $f_0(\frac{\epsilon}{D}, R_e)$ is only dependent on the relative pipe roughness.

For fully-developed turbulent flow, $R_e > R_{eft}$, where R_{eft} is the Reynolds number beyond which the fully-developed turbulent flow occurs,

$$R_{af} = \frac{D}{\alpha x f_0(\frac{\epsilon}{D}) G(R_{ew}, R_e)} \tag{A.24}$$

For partially-developed turbulent flow $(R_{et} < R_e < R_{eft})$

$$R_{af} = \frac{D}{\alpha x f_0(\frac{\epsilon}{D}, R_e) G(R_{ew}, R_e)} \tag{A.25}$$

Hence in turbulent flow regime R_{af} depends on location x, pipe geometry (pipe ID and pipe roughness), fluid properties, and inflow rates.

Appendix B. Wall Mass Transfer Effect on Friction Shears

B.1 Laminar Flow

Fully-developed laminar flow in a circular pipe exhibits a parabolic velocity profile (Figure B.1) if no mass transfer through the pipe wall exists,

$$u(r) = \frac{1}{4\mu}\frac{d\Phi}{dx}(r^2 - R^2) = 2U\left[1 - \frac{r^2}{R^2}\right] \tag{B.1}$$

where μ is the fluid viscosity, r the radial coordinate, Φ the flow potential defined by $\Phi = p + \rho g x \sin\theta$, and U the average velocity over a pipe cross section.
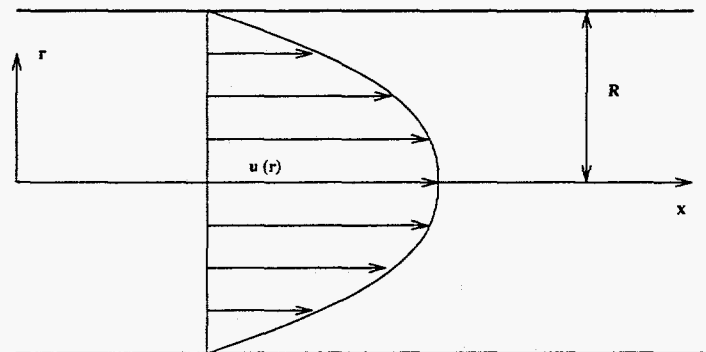

Figure B.1: Velocity Profile for the Fully-Developed Laminar Flow in Pipes

When mass transfer through the pipe wall exists, the parabolic velocity profile is inappropriate for describing the velocity distribution over the pipe cross section. As shown in Figure B.2, the velocity should increase for injection while decrease for suction following the law of mass conservation. Although fluid injection leads to the increasing of axial velocities across the whole pipe section, as can be imagined, the axial velocities near the pipe wall will increase more than those far away from the wall (and thus close to the centerline). Similarly, suction decreases axial velocities near the wall more significantly than those away from the wall. Therefore, it is expected that the velocity profiles shown in Figure B.2, where the axial velocities are normalized based on the average velocity U_0, can be rescaled into the profiles shown in Figure B.3 where the axial velocity is normalized by the average velocity U. U_0 is

37

the average fluid velocity where only the axial flow part flows in the pipe and no injection or suction are present, whilst U is the average axial velocity corresponding to the sum of axial flow and the flow through perforations. For three different cases with the same axial flow rate, one with injection, one with suction and the third with no injection or suction, it is easily seen that $U_{injection} > U_{no\ injection\ or\ suction} = U_0 > U_{suction}$.
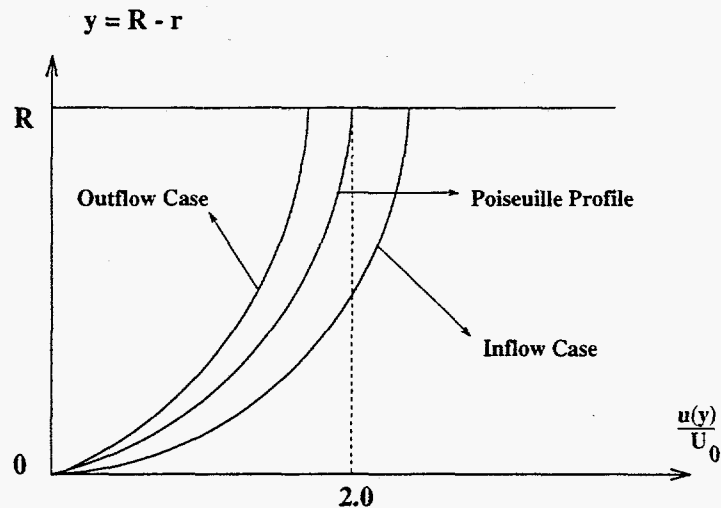
Figure B.2: Normalized Velocity Profile Based on the Average Axial Velocity

The expected profiles shown in Figure B.3 have been verified by numerical experiments of both Weissberg [35] and Hornbeck et al. [36]. Weissberg [35] found that the centerline values of the normalized axial velocities for injection and suction cases are equal to 1.7578 and 2.1523, respectively.

Figure B.3: Normalized Velocity Profiles Based on Local Average Velocity

In order to study the impact of injection or suction on pipe wall friction shear, it is

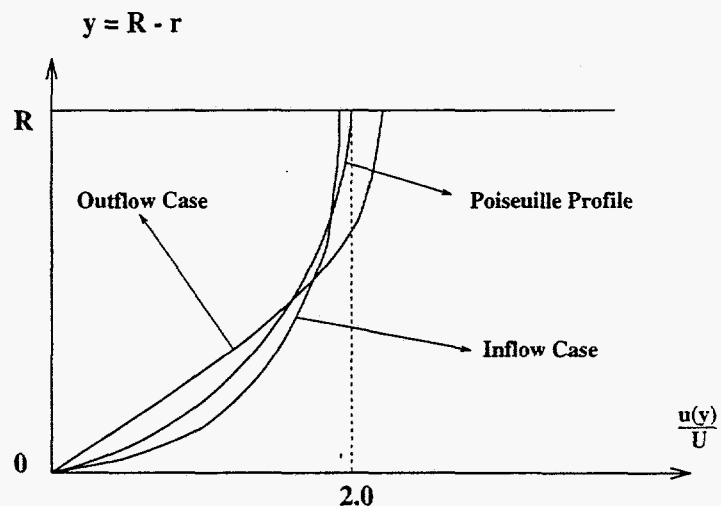necessary to analyse the normalized velocity profiles shown in Figure B.3. First let's look at the injection case. Suppose there exist two pipe flows, the first where both the axial flow and inflow are present, and the second where the total of both axial flow and inflow of the first case is flowing simultaneously only in the axial direction (i.e. no inflow). If the flows in both cases are fully developed, then the velocity profile for the first case should be the profile corresponding to injection in Figure B.3, whereas the velocity profile for the second case should be the Poiseuille one. Thus

$$\left[\frac{du(y)}{dy}\right]_{y=0,\ injection} > \left[\frac{du(y)}{dy}\right]_{y=0,\ no\ injection} \tag{B.2}$$

The wall friction shears are related to the fluid viscosity and velocity gradient at the pipe wall by

$$\tau_w = \mu\left(\frac{du}{dy}\right)_{y=0} \tag{B.3}$$

hence the wall friction shear for the first case (with injection) is larger than that for the second case (no injection). By using the definition of Fanning friction factor and noting the fact that the average velocities are equal for both cases, it can be concluded that

$$f_{injection} > f_{no\ injection} \tag{B.4}$$

i.e. , the injection leads to an increase of the wall friction shear and the Fanning friction factor.

By a similar arguments, it is not difficult to show that

$$\left[\frac{du(y)}{dy}\right]_{y=0,\ suction} < \left[\frac{du(y)}{dy}\right]_{y=0,\ no\ suction} \tag{B.5}$$

$$f_{suction} < f_{no\ suction} \tag{B.6}$$

Hence, for laminar pipe flow, injection increases the wall friction whereas suction decreases it. As an illustration, in the following the possible velocity profiles and their deviations from the Poiseuille distribution for the above-mentioned three different situations are considered. The velocity profiles can be expressed as:

- For axial flow without mass transfer through the pipe wall

$$u(r) = u_n(r) = u_{max}\left[1 - \left(\frac{r}{R}\right)^2\right] = 2U(2y_D - y_D^2) \tag{B.7}$$

- For axial flow with injection or suction

$$u(r) = u_w(r) = u_{max}y_D^m \tag{B.8}$$

where $y_D = y/R$, and m should be determined by matching experimental data. It is anticipated that

$$m \leq \tfrac{1}{2} \quad \text{(for the injection case)}$$
$$m \geq 1 \quad \text{(for the suction case)}$$

From Eq. B.7 and Eq. B.8, the average velocities can be calculated

$$U_n = \frac{1}{2} u_{max}$$

$$U_w = \frac{2u_{max}}{(m+1)(m+2)}$$

therefore, the deviation of velocity profile from parabolic (Poiseuille) distribution becomes

$$F(m, y_D) = \frac{u_w}{U_w} - \frac{u_n}{U_n} = y_D^m \frac{(m+1)(m+2)}{2} - 2(2y_D - y_D^2) \qquad (B.9)$$

The functional relationships among $F(m, y_D)$ and y_D as well as pipe wall mass transfer format (injection or suction) have been calculated and are shown in Figure B.4 and Figure B.5. These results can also be used to obtain velocity profiles of the types shown in Figure B.3.
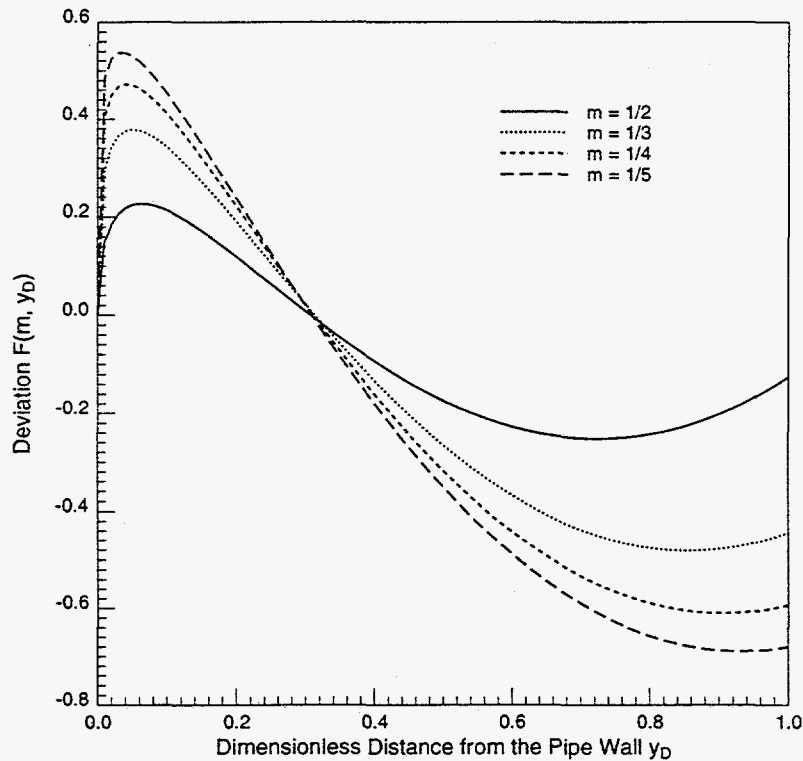

Figure B.4: Deviation from the Poiseuille Velocity Profile (Injection case)

Note that the effect of flow injection is to increase the wall friction shear of pipe flow. This behavior is contradictory to that found for flat plate laminar boundary layer flow, where the wall friction is reduced by fluid injection normal to the wall. The phenomenological

differences between these two kinds of flows are related to the effect of axial pressure gradient on flow dynamics. As pointed out by Kinney [15], in the case of boundary layer flow over a flat plate at zero incidence, the pressure gradient in the flow direction is zero, even in the presence of uniform injection through the plate wall. The situation is completely different for the case of laminar pipe flow with injection through the pipe wall. In the latter case, the axial pressure gradient is nonzero, and it is determined by the internal flow dynamics. Furthermore, the pressure gradient is also dependent upon the wall injection rate. Because the wall friction is intimately connected with the pressure gradient, as well as changes in the momentum flux in the flow direction, it is not unexpected that the frictional characteristics of laminar flat plate boundary layer and fully-developed internal flows would be quite different.
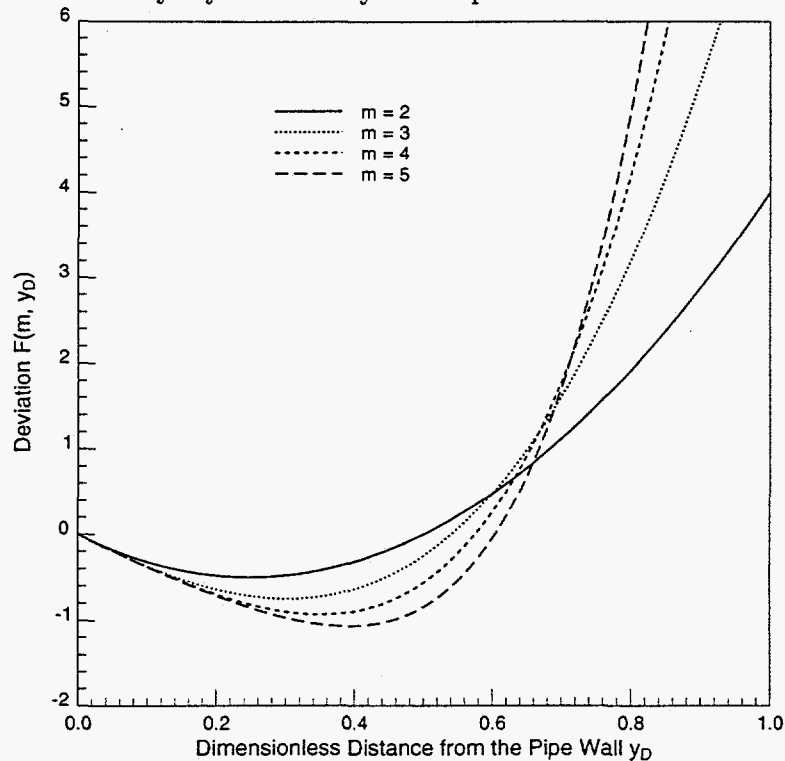

Figure B.5: Deviation from the Poiseuille Velocity Profile (Suction case)

In all the discussions above only the fully developed laminar flow is considered, i.e., we assume that the axial velocity u is only a function of the radial coordinate. This assumption is invalid for entrance flow or other non fully-developed laminar flows. In such situations, the axial velocity is a function of both the axial coordinate and the radial coordinate, $u = u(x, r)$, as a result the average velocity and the maximum velocity are dependent upon the axial coordinate x. The velocity profile development process occurs in a pipe where injection or suction through perforations exist. In a horizontal production well, starting at the toe, reservoir fluid flows into the wellbore and more and more fluids enter the wellbore from that point on. So an important question is: What well length is needed for flow in the wellbore to reach the fully-developed state? The work of Hornbeck et al. [36] for entrance flow in a porous pipe is briefly described here to answer the above question. By using a finite difference method, Hornbeck et al. [36] solved the steady-state Navier-Stokes equation and found that the development of fully-developed laminar flow is dependent on both the

inlet flow profile and the perforation flow format (i.e., injection or suction). Figure B.6 and Figure B.7 show sketches of Hornbeck et al. [36]'s results, where the abscissa represents the dimensionless axial position from the entrance point and the ordinate refers to the normalized dimensionless centerline axial velocity. Both figures show that the fully-developed laminar flow can be reached in a fairly short distance from the inlet and the building of the fully-developed laminar flow for parabolic inlet velocity profile case is much faster than that for the uniform inlet velocity profile case. For fluid flow in the wellbore, it is unlikely that the inlet velocity profile for each pipe segment is uniform, thus it can be expected that fully-developed flow may be assumed for the entire pipe where flow is laminar.
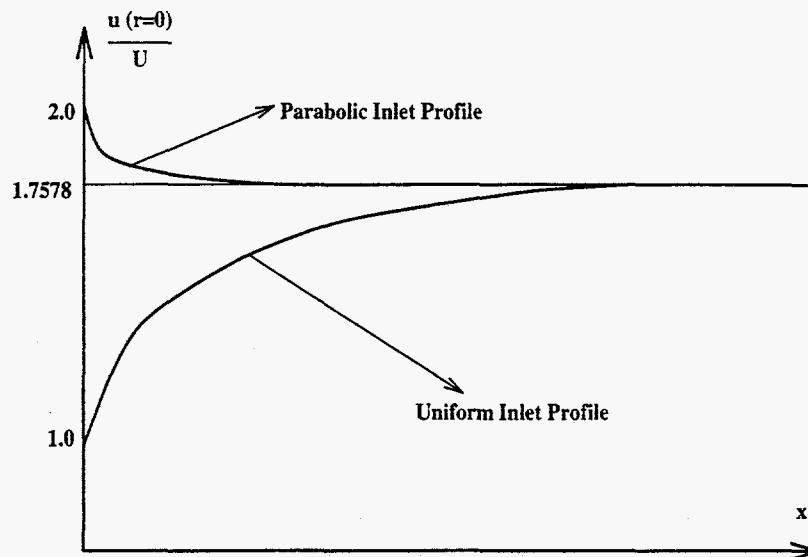

Figure B.6: Development of the Velocity Profile from Inlet with Injection through Pipe Wall

The case of pipe flow with suction needs special attention. Since part of the fluid flows out of the pipe through pipe wall, the velocity gradient near the pipe wall decreases along the axial direction (see Figure B.3), hence it is possible that at some point the velocity gradient near the wall may go to zero, resulting in zero wall friction. This point is usually known as the separation point. After the separation point, reverse flow near the wall occurs and the wall friction shear changes its direction and becomes favorable to axial flow.

For fully-developed laminar flow, both Kinney [15] and Raithby [22] found that the separation occurs at a certain suction Reynolds number. Kinney [15] stated that the separation suction Reynolds number is about -4.626 while Raithby [22] reported a value of -4.5978. Hornbeck et al. [36], Fredman & Gillis [37], Gupta [38] investigated the nonsimilar solution and proposed a separation point of $R_{ew} < -4.6$, where the gradient of the stream velocity in the radial direction goes to zero at the wall and reverse flow occurs for greater axial distances down the pipe. An experimental study performed by Quaile & Levy [39] supports these results. This value of separation suction Reynolds number is fairly small, and it can be easily exceeded in horizontal injection wells.
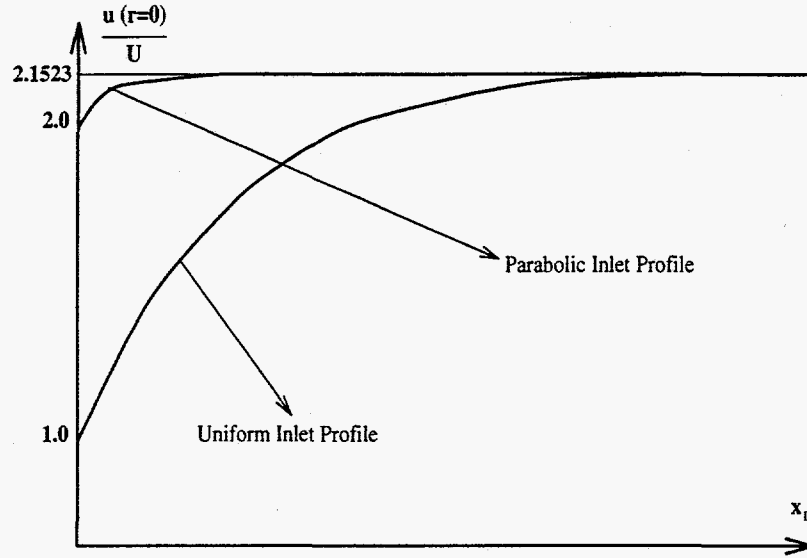
Figure B.7: Development of the Velocity Profile from Inlet with Suction through Pipe Wall

B.2 Turbulent Flow

It is commonly known that two major regions exist for turbulent pipe flow: the inner region and the outer region [40, 33]. The inner region is defined as that of the flow where the wall effects dominate and for smooth pipes the local velocity depends on the vairiables τ_w , ρ, ν and y only. The inner region can be further divided into three subregions:

- *The viscous sublayer.* This is the layer in the immediate neighbourhood of a pipe wall where the viscous shear dominates. Observations and experiments have shown that

$$u^+ = \frac{u}{u_\tau} = \frac{y u_\tau}{\nu} = y^+ \tag{B.10}$$

where the friction velocity u_τ is defined as $u_\tau = \sqrt{\frac{\tau_w}{\rho}}$, and the thickness of the viscous sublayer is determined by

$$y_1^+ = \frac{y_1 u_\tau}{\nu} = 5 \tag{B.11}$$

- *The buffer sublayer.* Further away from the pipe wall the turbulent velocity fluctuations (the Reynolds stress) start to contribute to the shear stress and there exists a region where the viscous and turbulent contributions are of equal importance. This region is known as the buffer sublayer and is determined by

$$5 < \frac{y u_\tau}{\nu} < 30 \tag{B.12}$$

thus the thickness of the buffer layer y_2 satisfies

43

$$y_2^+ = \frac{y_2 u_\tau}{\nu} = 30 \tag{B.13}$$

- *The logarithmic sublayer.* The Reynolds number for turbulent flow is usually very high, as a result the viscous sublayer and the buffer sublayer both occupy regions very close to the pipe wall. A third subregion dominated by the influence of pipe wall exists where the viscosity shear stress is much smaller than the Reynolds shear stress and thus can be neglected. This region is named the logarithmic sublayer and it can be easily shown that in this region the time-averaged velocity[1] satisfies the following equation

$$u^+ = A \ln y^+ + B \tag{B.14}$$

In the outer region, the velocity profile is strongly influenced by the upstream condition rather by the wall. For a typical boundary layer on an external surface the outer region might make up to 80 percent of the layer, whilst the remaining 20 percent could be considered as the wall region, or the inner region.

It has been found that the velocity profile in the fully-developed turbulent flow is accurately described over much of the pipe cross section by the logarithmic law (universal velocity profile). Departures from this law are only significant in a narrow region very close to the pipe wall and in the immediate vicinity of the pipe axis. Since these two regions make only a small contribution to the volumetric flow rate through any cross section of the pipe (velocity is small near the pipe wall, while the elemental area is small near the axis), the integration of the logarithmic law can be expected to provide a good estimate of the overall flow rate. Based on this assumption, the friction factor relation can be obtained by using the universal velocity profile and the definition of the friction velocity

$$f = \frac{\tau_w}{\frac{1}{2}\rho U^2} = 2\left(\frac{u_\tau}{U}\right)^2 \tag{B.15}$$

$$f^{-0.5} = A_1 \ln(R_e f^{0.5}) + B_1 \tag{B.16}$$

where

$$A_1 = \frac{A}{\sqrt{2}}$$

$$B_1 = \frac{1}{\sqrt{2}}[B - A(1.5 + \ln(2\sqrt{2}))] = \frac{1}{\sqrt{2}}[B - 1.5A(1 + \ln 2)]$$

Substituting $A = 2.5$, $B = 5.5$, the following friction factor correlation is obtained

$$f^{-0.5} = 1.768\ln(R_e f^{0.5}) - 0.60 = 4.07\log(R_e f^{0.5}) - 0.60 \tag{B.17}$$

---

[1]The time-averaged velocity is used here to distinguish from the space-averaged velocity across a pipe cross section. Even for steady-state turbulent flow, velocity still changes with time and space, however, it is only slightly different from the time-averaged velocity, which does not change with time. The velocity fluctuation is quite small but changes with time. It is the fluctuation part that contributes significantly and nontrivially to the shear stress and makes the turbulent flow problem extremely complicated.

44

It is found that a better correlation of the experimental data over the full Reynolds number range of turbulent flow can be obtained by modifying the constants A_1 and B_1

$$f^{-0.5} = 1.74 \ln(R_e f^{0.5}) - 0.40 = 4.0 \log(R_e f^{0.5}) - 0.40 \qquad (B.18)$$

Eq. B.18 is known as the Prantdl universal friction law (Ouyang & Aziz, [26]) and has been verified as the best correlation for the friction factor for smooth pipes.

The pipe roughness is an important factor affecting the wall friction shear for turbulent flow. The manner in which the pipe roughness affects the flow and the friction shear depends on the relative magnitude of the surface roughness ϵ, the thickness of the viscous sublayer y_1 and the thickness of the buffer sublayer y_2 found in smooth pipes as described below [40]:

- If the pipe roughness is less than the thickness of the viscous sublayer, then the flow outside the viscous sublayer is found to be entirely unaffected by the presence of the pipe roughness and the flow behaves as though the pipe surface were completely smooth. This region is defined as the fluid-dynamically smooth region. The criterion for the fluid-dynamically smooth region is

$$\frac{\epsilon u_\tau}{\nu} \le y_1^+ = 5 \qquad (B.19)$$

- If the pipe roughness exceeds significantly the thickness of the buffer sublayer, a major part of each roughness element is exposed to the mean velocity profile, which is independent of the fluid viscosity. The wall friction shear stress is thus completely caused by the pressure drag on the individual roughness elements and it is not dependent upon the fluid viscosity and thus the Reynolds number. This regime is termed the fluid-dynamically rough regime, or the fully–developed turbulent flow regime. This region shows up when the pipe roughness is much greater than about two times the thickness of the buffer sublayer, i. e.

$$\frac{\epsilon u_\tau}{\nu} \ge \frac{2y_2 u_\tau}{\nu} \approx 70 \qquad (B.20)$$

- If the pipe roughness is between the two limits defined in Eq. B.19 and Eq. B.20, the flow exhibits some of the characteristics of both the fluid-dynamically smooth regime and the fluid-dynamically rough regime. In this regime, the wall friction shear is related to both the Reynolds number and the pipe roughness. This regime is known as the intermediate regime or the partially-developed turbulent flow regime.

The velocity profile for smooth or rough pipe flows can be expressed in the from

$$\frac{u}{u_\tau} = A \ln \left(\frac{y}{\epsilon} \right) + h \left(\frac{\epsilon u_\tau}{\nu} \right) \qquad (B.21)$$

This relationship is more general in the sense that it applies to the fluid-dynamically smooth and rough regimes, as well as to the intermediate regime. In the smooth and rough regimes, the function h is independent of the form of the surface roughness, but in the

intermediate regime, the value of h depends on the roughnes pattern. For example, sand-roughened pipes and commercial pipes having the same relative roughness have different values of h in the intermediate regime.

The functional form of h is

$$
h\left(\frac{\epsilon u_\tau}{\nu}\right) = \begin{cases} A\ln\left(\dfrac{\epsilon u_\tau}{\nu}\right) + B & (smooth) \\[2mm] 8.5 & (rough) \\[2mm] 5.45 - 4\sqrt{2}\log\left[\dfrac{1.25}{\sqrt{2}}\dfrac{\nu}{\epsilon u_\tau} + \dfrac{1}{3.7}\right] & (intermediate) \end{cases} \tag{B.22}
$$

From the velocity profile (Eq. B.21) the following friction factor equation can be derived:

$$
\left(\frac{2}{f}\right)^{0.5} = A\ln\left(\frac{D}{\epsilon}\right) + h\left(\frac{\epsilon u_\tau}{\nu}\right) - 1.5A - A\ln 2 \tag{B.23}
$$

It has also been shown that a value for h of about 8.62 rather than 8.5, and $A = 2.46$ rather than 2.5 can lead to a better match with experimental data for rough pipes. Substituting function $h(\frac{\epsilon u_\tau}{\nu})$ into Eq. B.23, the following friction factor correlation is thus obtained

$$
\left(\frac{2}{f}\right)^{0.5} = \begin{cases} A\ln(R_e f^{0.5}) + B - 1.5A(1.0 + \ln 2) & (smooth) \\[2mm] A\ln\left(\dfrac{D}{\epsilon}\right) + 8.62 - 1.5A - A\ln 2 & (rough) \\[2mm] -4\sqrt{2}\log\left[\dfrac{1.25}{R_e f^{0.5}} + \dfrac{\epsilon}{3.7D}\right] & (intermediate) \end{cases} \tag{B.24}
$$

As mentioned above, the shear stress is composed of two main components, viscous and turbulent (Reynolds) (Figure B.8)

$$
\tau = \tau_{vis} + \tau_{tur} = \mu\frac{\partial u}{\partial y} - \rho\overline{u'v'} \tag{B.25}
$$

For flow in pipes, it can be shown that the shear stress distribution is proportional to the distance from the pipe wall for turbulent flow as well as for laminar flow. The turbulent shear goes to zero at the wall since the velocity fluctuation is zero at the wall, whereas the viscous shear is nonzero only in a very thin region $(y < y_2)$, which is a combination of the viscous sublayer and the buffer sublayer. Note that the turbulent shear reaches a maximum value near the pipe wall.

Based on the above analysis, it is not difficult to see that the wall friction shear stress is dependent on the fluid viscosity and the time average velocity profile near the pipe wall,

$$
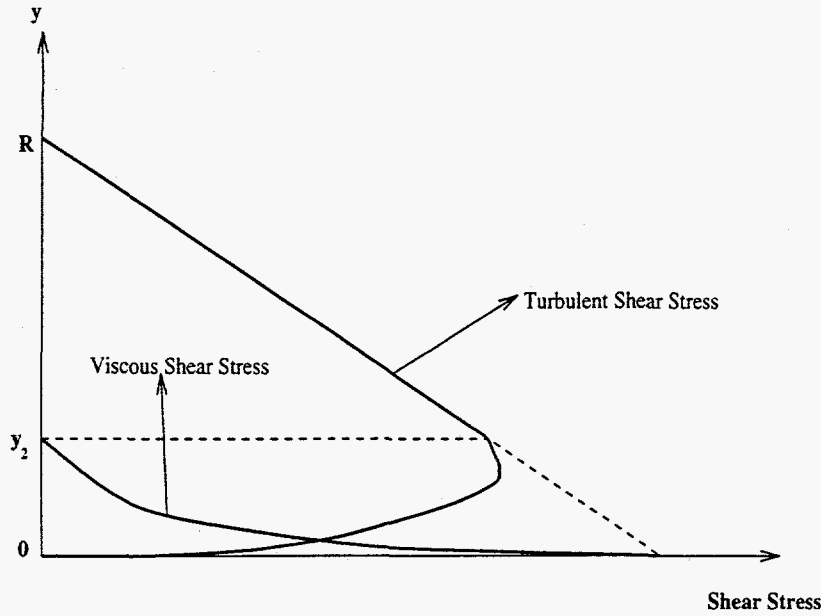\tau_w = \mu\left(\frac{\partial u}{\partial y}\right)_{y=0} \tag{B.26}
$$

46

Figure B.8: Shear Stress Chnage with the Radial Distance from the Pipe Centerline

The time-averaged velocity profile for turbulent flow can be represented by a power-law relationship

$$\frac{u}{U_\infty} = \left(\frac{y}{R}\right)^{\frac{1}{n}} \tag{B.27}$$

if y is greater than the turbulent boundary thickness, δ, the time average velocity will be very close to the maximum velocity (centerline velocity). By adjusting the power index n, Eq. B.27 can match the measured velocity profile for Reynolds number between 4000 and 3×10^6 . From this relationship the wall friction shear stress can be derived

$$\tau_w = \frac{1}{2}\rho U^2 K (R_e)^{-2/(n+1)} \tag{B.28}$$

where K is a constant dependent on the power index n and the average velocity u over the pipe cross section.

Correspondingly, the Fanning friction factor becomes

$$f = K(R_e)^{-2/(n+1)} \tag{B.29}$$

This equation is termed as the $\frac{1}{5}$th, $\frac{1}{6}$th, $\frac{1}{7}$th, $\frac{1}{8}$th and $\frac{1}{9}$th power law relationship for $n = 5, 6, 7, 8$ and 9 respectively. As shown by Ouyang & Aziz [26], various power-law friction factor relationships are valid for specific Reynolds number ranges.

With the presence of mass transfer through perforations, the time average velocity profile is altered due to the interaction between the axial flow and the perforation flow. For the injection case, the inflow lifts and expands the turbulent boundary layer and thus increases the axial velocity beyond the layer while decreases the velocity within the layer to follow the mass conservation law (Figure B.9). As a consequence the axial velocity gradient near the pipe wall decreases and so does the wall friction shear stress. On the contrary, the suction lowers and reduces the boundary layer and thus decreases the average velocity

outside the layer but increases the velocity inside the layer, and results in an increase of the axial velocity gradient near the pipe wall and hence the wall friction shear stress. This analysis is consistent with the numerical observations of Kinney & Sparrow [17] for pipe flow with suction through the pipe wall.
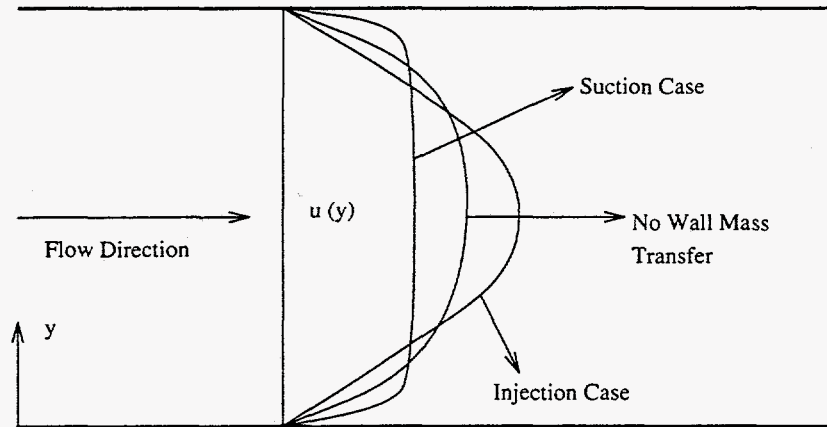

Figure B.9: Velocity Profile Change due to Injection or Suction through the Pipe Wall